

Jamming III: Characterizing Randomness via the Entropy of Jammed Matter

Christopher Briscoe, Chaoming Song, Ping Wang, Hernán A. Makse

¹ *Levich Institute and Physics Department, City College of New York, New York, NY 10031, US*

(Dated: September 24, 2009)

The nature of randomness in disordered packings of frictional and frictionless spheres is investigated using theory and simulations of identical spherical grains. The entropy of the packings is defined through the force and volume ensemble of jammed matter and shown difficult to calculate analytically. A mesoscopic ensemble of isostatic states is then utilized in an effort to predict the entropy through the definition of a volume function dependant on the coordination number. Equations of state are obtained relating entropy, volume fraction and compactivity characterizing the different states of jammed matter, and elucidating the phase diagram for jammed granular matter. Analytical calculations are compared to numerical simulations using volume fluctuation analysis and graph theoretical methods, with reasonable agreement. The entropy of the jammed system reveals that the random loose packings are more disordered than random close packings, allowing for an unambiguous interpretation of both limits. Ensemble calculations show that the entropy vanishes at random close packing (RCP), while numerical simulations show that a finite entropy remains in the microscopic states at RCP. The notion of a negative compactivity, that explores states with volume fractions below those achievable by existing simulation protocols, is also explored, expanding the equations of state. The mesoscopic theory well reproduces the simulations results in shape, though a difference in magnitude implies that the entire entropy of the packing may not be captured by the herein presented methods. We discuss possible extensions to the present mesoscopic approach describing packings from RLP to RCP to the ordered branch of the equation of state in an effort to understand the entropy of jammed matter in the full range of densities from RLP to FCC.

I. INTRODUCTION

Granular materials fall under the scope of athermal systems, which includes glasses, colloids and gels, among others. These athermal systems exhibit non-equilibrium behavior, such that equilibrium statistics is insufficient in its attempt to describe the system dynamics. These systems are thereby considered "complex", and their characterization finds application in fields from chemistry to fluid mechanics and beyond. For granular systems, in particular, a phase transition [1, 2] occurs when granular materials are compressed such that they develop a nonzero stress in response to a strain deformation [3, 4, 5, 6, 7]. This transition, referred to as the *jamming transition*, occurs at a critical volume fraction, ϕ_c , depending on interparticle friction and preparation protocol. Analysis of the jamming transition produces a phase diagram of jammed granular matter for identical spheres, characterized by ϕ_c and the average mechanical coordination number [8].

The existence of boundaries in the phase diagram of [8] are related to well-defined upper and lower limits in the density of disordered packings; random close packing (RCP) and random loose packing (RLP) [9, 10]. How to properly define RCP and RLP remains a longstanding open question in the field. It has been suggested [1] that treating a jammed system via the volume (V) ensemble introduces an analogue to temperature in equilibrium systems. This analogue, "compactivity", is a measure of how compact a system could be. Within this framework [1, 8], RCP is achieved in the limit of minimal compactivity and RLP is achieved in the limit of maximal compactivity. Therefore, the boundaries of a

phase diagram for jammed matter could be defined by the limits of zero and infinite compactivities.

In order to approach jammed systems with a statistical ensemble approach, a definition of RCP and RLP requires proper definitions of jammed states and the concept of randomness [11]. In an attempt to rigorously define jammed states, Torquato and coworkers have proposed three categories of jamming [12]: locally, collectively and strictly jammed. This definition is based purely on geometrical considerations and therefore it is only sufficient for frictionless grains. Frictional systems incorporate geometrical constraints but are dominated by inter-particle normal and tangential contact forces [13]. In Fig. 1 we see a hard sphere system is not locally jammed if only normal forces are considered, since the ball can freely move in the vertical direction. The same geometrical configuration is locally jammed if friction is allowed between the particles, revealing the importance of forces in the definition of jamming for frictional particles. Therefore, a definition of the jammed state for granular materials considering only geometrical constraint is insufficient to describe frictional grains.

Frictional systems further exhibit an inherent path dependency, as granular contacts between grains result in the loss of energy conservation. Approaches based on the potential energy landscape [7] thereby cannot be used for granular materials, as such a potential does not exist for the non-conservative frictional contact force. In this study, our framework is based on statistical mechanics [14], defining the jammed state at the V-ensemble supplemented by force and torque balance conditions, wherein volume replaces energy as the conservative quantity for a statistical ensemble. The free volume associated with each particle in the packing is calculated as a function

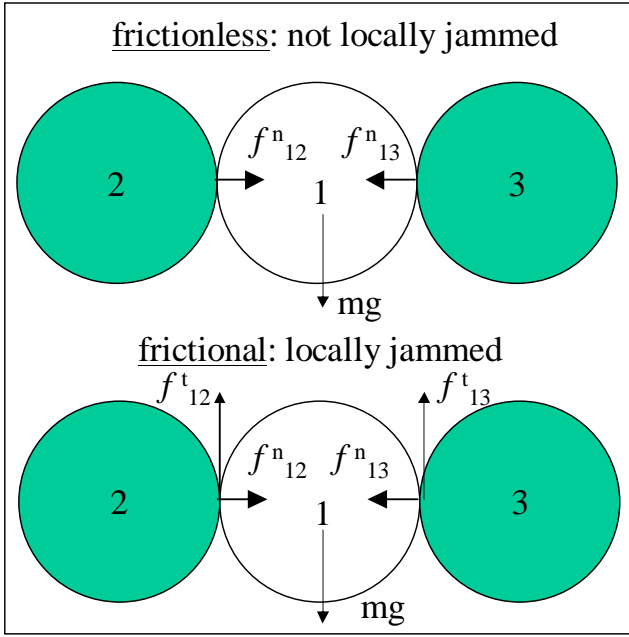


FIG. 1: (a) The inset shows a ball in 2d under mechanical equilibrium by two nearest neighbor contacts. The ball is not jammed under a normal force interaction. It jams when tangential forces are present.

of the geometrical coordination number using a coarse-grained mesoscopic theory of quasi-particles. This allows one to define the RLP and RCP states through the ensemble of isostatic states.

Randomness in statistical systems is typically characterized by the entropy, the equation of state derived from the number of microstates available to the system. In equilibrium statistical mechanics, entropy provides the link between these microstates and the macroscopic thermodynamic properties of the system. We explore that the concept of randomness is well-defined for the V-ensemble following the Gibbs distribution [14], and is different from the measurement of randomness of single packing in term of the ensemble of order parameters proposed in [11]. Therefore, calculating the entropy within the V-ensemble can relate the available microscopic volume for each grain to the macroscopic system properties, such as volume fraction, average coordination number, and compactivity, in the case of frictional hard spheres.

We first investigate frictional packings of equal sized spheres at the jamming transition generated via computer simulations. As the volume fraction approaches the jamming transition from above, $\phi \rightarrow \phi_c^+$, the system approaches the isostatic condition and observables are shown to scale with the distance from the jamming transition as a power law of $\phi - \phi_c$ [4, 6, 7], including stress, average coordination number and elastic moduli. We therefore consider the jamming transition as the limit at which the stress tends to zero and the average coordination number tends to a finite, non-zero, value. Mechanical equilibrium imposes an average mechanical co-

ordination number, Z , larger or equal than the minimum isostatic coordination as conjectured by Alexander [15] (see also [4, 5, 7, 13, 16, 17, 18, 19]). The ensemble of packings at the jamming transition explores the phase diagram of jammed matter by assuming the system is exactly isostatic at the transition, and that the isostatic condition varies as a function of the inter-particle friction coefficient [8].

We compute the equations of state, entropy and compactivity, as a function of volume fraction, ranging from RLP to RCP. The entropy is calculated by two methods. First, a direct analysis of volume fluctuations via Einstein Fluctuation theory explores the clustering of microscopic volumes. Second, graph theoretical methods using the Shannon entropy analyze the network forming properties of the granular system. These simulations reveal that random loose packings have a higher disorder than random close packings. Further, packings approaching RLP have a higher compactivity than those approaching RCP.

Then we perform theoretical calculations under the quasi-particle mesoscopic approximation of [8], where a coarse-graining over a mesoscopic length scale of several particle diameters is implied, giving rise to a mesoscopic configurational entropy, achieving a minimal value at the volume fraction of RCP and maximal value at the RLP limit. The results define RCP and RLP at the mesoscopic level in general agreement with simulations, suggesting that the concept of randomness in [14] together with the notion of the jammed state in [8] are useful. The numerical results further suggest that the mesoscopic entropy requires augmentation to include the entropy of the microscopic states neglected at the mesoscopic level.

The maximal volume fraction for jammed spheres in 3d created using purely random protocols occurs at $\phi_{\text{RCP}} \simeq 0.64$. Packings above RCP exist with some degree of order, up through the perfectly ordered FCC state with $\phi_{\text{FCC}} = 0.74$ in 3d. It is of interest to understand how one would expand the existing mesoscopic theory to include all packings from RLP to FCC, and what effect this would have at the transition between disordered and ordered packings at RCP. While entropy tends to zero as we approach FCC, the existing mesoscopic theory considers entropy minimal at RCP, accounting only for disordered states. It remains an open topic as to whether a phase transition occurs at RCP, noted by a discontinuous change in the equations of state, or whether disorder decays smoothly when approaching FCC. We discuss plausible scenarios to rationalize the transition between RCP and FCC as the volume fraction is increased by partial crystallization. We speculate that at RCP a thermodynamic transition, either continuous or discontinuous, may occur. Such a transition can be described by a full theory that includes both ordered and disordered states and is beyond the scope of the present work. We stress that this is a hard sphere transition different from the jamming transition obtained for deformable particles as the external pressure approaches zero. In this work,

hard sphere packings are numerically realized by simulating soft particles in the limit of zero pressure using the “split” algorithm explained in Section II.A [4, 5, 8].

Existing packing protocols exploring jammed packings may not probe the entire phase diagram for jammed matter, as packings with a negative compactivity may exist with volume fractions beneath the minimum value [20]. The mesoscopic theory is analyzed in an effort to characterize these packings that are inaccessible via random generation protocols.

II. SIMULATIONS AND RESULTS

A. Packing Preparation

First, we investigate the entropy of jammed granular matter by analyzing computer generated packings of 10,000 spherical equal-size particles (a reader familiar with [8] can refer to section II.C).

Two spherical grains in contact at positions \vec{r}_1 and \vec{r}_2 and with radius R interact with a Hertz normal repulsive force [21] and Mindlin tangential contact forces [22].

The Hertz force is defined as:

$$F_n = \frac{2}{3} k_n R^{1/2} \delta^{3/2}, \quad (1)$$

and an incremental Mindlin tangential force is defined as:

$$\Delta F_t = k_t (R\delta)^{1/2} \Delta s, \quad (2)$$

Here the normal overlap is $\delta = (1/2)[2R - |\vec{x}_1 - \vec{x}_2|] > 0$. The normal force acts only in compression, $F_n = 0$ when $\delta < 0$. The variable s is defined such that the relative shear displacement between the two grain centers is $2s$. The prefactors $k_n = 4G/(1 - \nu)$ and $k_t = 8G/(2 - \nu)$ are defined in terms of the shear modulus G and the Poisson’s ratio ν of the material from which the grains are made. We use $G = 29$ GPa and $\nu = 0.2$ typical values for spherical glass beads and we use $R = 5 \times 10^{-5}$ m and the density of the particles, $\rho = 2 \times 10^3$ kg/m³. Viscous dissipative forces are added at the global level affecting the total velocity of each particle through a term $-\gamma\vec{x}$ in the equation of motion, where γ is the damping coefficient related to the viscosity of the medium $\eta = \gamma/(6\pi R)$. These dissipative forces ensure that the granular system cannot ‘rattle’ forever. We measure the time in units of $t_0 = R\sqrt{\rho/G}$, the compression rate in units of $\Gamma_0 = 5.9t_0^{-1}$ and the viscosity in units of $\eta_0 = 8.2R^2\rho/t_0$. The dynamics follows integration of Newton’s equations.

Sliding friction is also considered:

$$F_t \leq \mu F_n. \quad (3)$$

That is, when F_t exceeds the Coulomb threshold, μF_n , the grains slide and $F_t = \mu F_n$, where μ is the static friction coefficient between the spheres.

The critical volume fraction at the jamming transition, ϕ_c , is achieved by the “split” algorithm as explained in [8], allowing one to obtain packings at the critical density of jamming with arbitrary precision.

Initially, a dilute particle configuration is generated randomly, usually with a volume fraction $0.30 \sim 0.36$. Then, an extremely slow isotropic compression, without friction, is applied to this configuration until the system reaches ϕ_i in an unjammed state. For frictional packings the critical volume fraction, ϕ_c , is such that $\phi_c < 0.64$. Additionally, the mechanical coordination number, Z , or the number of contacts for a given particle which apply a force to maintain the jamming condition at ϕ_c , is $Z < 6$ for frictional systems. Therefore, the system now at ϕ_i is allowed to relax while maintaining the frictionless condition, such that the system is unable to achieve jamming. Z and the pressure decay to zero as we relax the system below jamming.

After obtaining the relaxed, unjammed and frictionless state with initial volume fraction ϕ_i , a particular μ is given to the particles and compression is applied with a compression rate Γ until a given volume fraction ϕ_1 . Then the compression is stopped and the system is allowed to relax to mechanical equilibrium by following Newton’s equations without further compression. The split algorithm searches for ϕ_c by setting upper and lower boundaries for ϕ_c and dividing the size of those boundaries in half by iteratively compression (or expanding) the system, followed by relaxing and then testing for a non-zero stress in the system, as outlined in [8]. This numerical process is repeated for packings with varying ϕ_i along the range of μ between 0 and ∞ . The results fill a phase diagram for jammed identical spheres right at the jamming transition as obtained in [8] and shown in Fig. 2.

The friction coefficient ranges from 0 to ∞ producing packings with coordination number varying from $Z \approx 6$ to $Z \approx 4$, respectively. We find that there exists a common function $Z(\mu)$ over the different Γ and ϕ_i (see [8]). For $\mu \rightarrow \infty$, ϕ ranges from the RLP limit $\phi_{\text{RLP}} \approx 0.55$ obtained when $\Gamma \rightarrow 0$ and $\phi_i < 0.55$ to the RCP limit $\phi_{\text{RCP}} \approx 0.64$ obtained for larger Γ and $\phi_i \rightarrow 0.64$. For $\mu = 0$, the density is approximately $\phi \approx \phi_{\text{RCP}}$ with $Z \simeq 6$. All of the packings used herein, along with the computer codes necessary to generate the packings and calculate their entropy can be downloaded at <http://jamlab.org>.

B. Phase Diagram

Simple counting arguments, neglecting correlations between nearest neighbors, consider that a necessary condition for mechanical equilibrium is that the number of independent force variables must be larger or equal than the number of linear independent force/torque balance equations. Alexander [15] conjectured that at the transition point for frictionless spherical packings [6, 15, 17] the

system is exactly isostatic with a minimal coordination, $Z = 2d = 6$ in 3d. Such a conjecture can be extended to the infinite friction case, where $Z = d + 1 = 4$ [1, 6]. In the presence of finite inter-particle friction coefficient μ , there exists a dependency of Z and μ suggested by simulations [8, 13, 16].

Figure 2 shows the phase diagram used for all equation of state calculations presented herein, as obtained using the "split" algorithm as described above in the plane (ϕ_c, Z) (for simplicity, in what follows we denote $\phi = \phi_c$). That is, we understand that all packings considered herein are at the jamming transition and are hard sphere packings). As discussed in [8], packings along the RCP line for finite μ are most difficult to obtain, most notably near C point in Fig 2, resulting in higher values of the lowest achievable stress for those packings. The G-line, at $Z = 4.0$, indicates the theoretical Z for infinite friction packings. The grey line at $Z = 4.2$ indicates the approximate lowest achievable Z possible using the present "split algorithm". The solid color lines in Fig. 2 are averages used in all following calculations. Near the RLP and RCP lines for a some fixed μ , we observe notably higher values of Z . These values are not included in the average. This allows us to use a constant value as an approximation for the mechanical coordination number.

We compare this result to the phase diagram as predicted by theoretical model asserted in [8]. Note that the isostatic condition [15] predicts $Z = 6$, while Fig. 2 includes packings with $6 < Z \leq 6.2$, and $\phi > 0.634$ as predicted by the theory for RCP. We suggest that these packings are new microstates of jammed matter (indicated by the shaded portion of the phase diagram) which are not accounted for in the mean-field version of [8, 23]. While they remain a component of the ensemble generated via the above described simulation protocol, their existence remains a topic of ongoing study.

C. Entropy from Voronoi Volume Fluctuations

In the absence of energy conservation, a different statistical approach is necessary to describe the ensemble properties of jammed granular matter. Along this line of research, Edwards [14] proposes replacing the system energy by the volume as the conservative quantity such that a microcanonical partition function of jammed states can be defined and a statistical mechanical analysis is plausible. Therefore, a microscopic volume must be associated with each grain.

As detailed in Jamming I [23], the definition of a Voronoi cell is a convex polygon whose interior consists of all points closer to a given particle than to any other. Further, it is additive and tiles the system volume completely. The formula for the Voronoi volume of a particle, i , in terms of particle positions for monodisperse spheri-

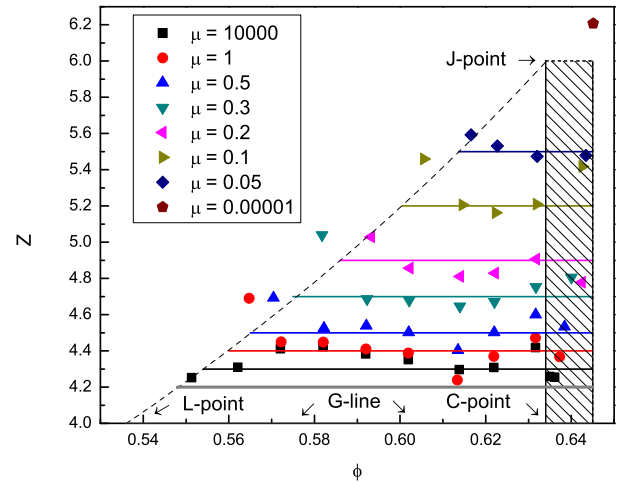


FIG. 2: The phase diagram of jamming from simulation results. We use the same algorithm to generate the packings as done in [8]. Here, we use 10,000 particles, while in [8] only 1000 were used. A larger number of particles is necessary for accurate entropy calculations. The volume fraction is denoted by ϕ as opposed to ϕ_c for simplicity. Horizontal lines show the average coordination number used for packings of constant μ . The dashed line represents the theoretical RLP line. The solid vertical line at $\phi = 0.634$ is the theoretical RCP line obtained in [8]. Notice that some packings exist to the right of the RCP line. Such packings are not captured by the theory, indicating that microscopic fluctuations beyond the mesoscopic theory of [8] are important close to the RCP state. The solid grey line at $Z = 4.2$ indicates the lower limit for Z available using the present split algorithm. The J-point, located at $(\phi, Z) = (0.634, 6)$, is the theoretical frictionless jamming point. The L-point, located at $(\phi, Z) = (0.536, 4)$, is the theoretical jamming point for $\mu \rightarrow \infty$ with $X \rightarrow \infty$. The C-point, located at $(\phi, Z) = (0.634, 4.0)$, is the theoretical jamming point for $\mu \rightarrow \infty$ with $X \rightarrow 0$. The G-line, $Z = 4.0$ is the theoretical average Z achieved for all infinite friction packings of identical spherical grains in 3d.

cal packings in 3d is [23]

$$\mathcal{W}_i^{\text{vor}} = \frac{1}{3} \int \left(\frac{1}{2R} \min_j \frac{r_{ij}}{\cos \theta_{ij}} \right)^3 ds, \quad (4)$$

where \vec{r}_{ij} is the vector from the position of particle i to that of particle j , the integrand is over all the directions \hat{s} forming an angle θ_{ij} with \vec{r}_{ij} , and R is the radius of the grain. The Voronoi volume is used to tile the total system volume, and replaces energy as the conserved quantity in a new micro-canonical ensemble for jammed granular matter. Therefore, fluctuations in Voronoi cell volumes are related to the compactivity of the jammed system, much like energy fluctuations are directly related to the system temperature in equilibrium thermodynamics. We notice that the Voronoi-Delaunay decomposition is the basis for Hales proof of the Kepler conjecture [24]. Below, we treat the monodisperse case. Other cases will be treated in subsequent papers.

Next, we calculate the entropy of the numerical pack-

ings in Fig. 2 from Voronoi volume fluctuation analogous to Einstein Fluctuation theory. We first define the Voronoi cell associated with each particle i and calculate its Voronoi volume \mathcal{W}_i . Calculation of a Voronoi cell volume begins by defining the polygon between two Delaunay contacts, having finite number, m , vertices. Two grains are considered Delaunay contacts if their corresponding Voronoi cells share a face. Delaunay contacts are determined by the network of grain positions and radii calculated using QHull software, available at <http://www.qhull.org>. The contribution of this polygon to calculating the Voronoi volume comes from the ability to associate a pyramid, comprised of the center of each particle as the apex, and the m -sided polygon as its base, as shown in Fig. 3 (schematically in 2d for simplicity), to each particle. The two pyramids are symmetric. The volume of this pyramid is the contribution to the Voronoi volume of the cell surrounding a particle, exclusive to the particular Delaunay contact which shares the polygon base. Repeating this process for each Delaunay contact results in the complete Voronoi volume surrounding a particle. The Voronoi volume is thereby the microscopic volume associated with each grain.

We perform statistical analysis of the volume fluctuations by considering a cluster of n particles. The Einstein fluctuation relation is defined as follows [25, 26]:

$$\sigma_n^2 \equiv \langle (\mathcal{W}_n - \langle \mathcal{W}_n \rangle)^2 \rangle = \lambda X^2 d \langle \mathcal{W}_n \rangle / dX \quad (5)$$

Equation (5) is analogous to equilibrium thermodynamics, replacing energy and temperature by volume and compactivity, X , in the Edwards picture. Note that λ is the analogue of the Boltzmann constant k_B that defines the units of compactivity.

We calculate the average volume, $\langle \mathcal{W}_n \rangle$ and fluctuations $\sigma_n \equiv \langle (\mathcal{W}_n - \langle \mathcal{W}_n \rangle)^2 \rangle$, where $\langle \cdot \rangle$ is an average over many n -clusters. From the large n behavior we extract the fluctuations versus volume fraction, ϕ , for every packing depicted in Fig 2. Figure 4 shows the fluctuations as a function of n for packings with infinite friction, displaying the largest range of volume fractions in the data used herein. We find that for sufficiently large $n \gg n_c$, the fluctuations scale with n and therefore are extensive and well-defined.

Figure 5 shows the approximate value of n_c at which the extensive nature of the fluctuations reaches its maximal value, as a function of ϕ . Lower volume fractions, approaching RLP, require higher values of $n \approx 1000$ to achieve this condition. This result contrasts with the results of [27], although there the system was smaller, $N \approx 100$, and two-dimensional. Reference [27] acknowledges that if grain volumes can be treated as independent random variables, then the fluctuation in clusters of n Voronoi cell volumes should scale with n . For clusters of jammed grains, this was not observed in [27], indicating the existence of correlations between the Voronoi cell volumes within a cluster. However, in the present study, the value of n at which the fluctuations are extensive is

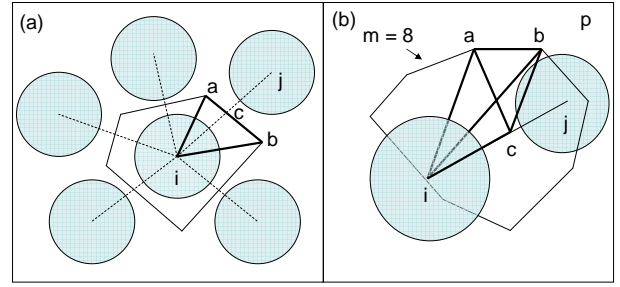


FIG. 3: (a) Example of 2d Voronoi cell - All of the calculations are done in 3d but are shown here in 2d for simplicity. The line between the centers of particles i and j is defined by \overline{ij} , equivalent to r_{ij} . The line perpendicular to the bisection of \overline{ij} is defined by \overline{ab} , intersecting \overline{ij} at point c . 4 additional particles are Delaunay contacts of particle i , such that a 5 sided polygon (pentagon) surrounds particle i by virtue of intersecting bisecting lines between each pair of Delaunay contacts. Points a and b are defined as the boundary of the Voronoi cell line between particles i and j . A triangle is thereby formed by points i and \overline{ab} , the area of which is the contribution of the Voronoi cell of particle i exclusive with its Delaunay contact to particle j . This process is repeated for all Delaunay contacts of i to give the entire Voronoi cell area. Note that a symmetric area to Δiab exists as Δjab , and can be applied to the Voronoi cell area of particle j . (b) Example of 3d Voronoi cell - The line between the centers of particles i and j is defined by \overline{ij} , equivalent to r_{ij} . The plane perpendicular to the bisection of \overline{ij} is defined by p , intersecting \overline{ij} at point c . Note that particles i and j are identical spheres, with particle j appearing smaller only to illustrate the 3d properties of the system. Plane p is intersected by m other planes, creating an m -sided polygon between particles i and j . Each plane intersecting plane p (not shown) is a plane bisecting \overline{ik} , the line between the centers of particle i (or j) and another particle k in the system, where k is one of m particular particles. A pyramid is thereby formed using the m -sided polygon as the base, and i (or j) as the apex. This pyramid is symmetric over plane p , and its volume is the contribution to the Voronoi volume of particle i from particle j , or vice versa, exclusively. The volume of the pyramid is calculated by separating the pyramid into 8 smaller pyramids, using the triangle composed of one of the m available sides, and \overline{c} as its base and i as its apex. This is illustrated by using \overline{ab} and c as the base of a pyramid with apex i . The volume of this pyramid is calculated and the process is repeated for each of the m sides, adding each obtained volume to the Voronoi volume of both i and j . The entire process is then repeated for all Delaunay contacts for a given particle, resulting in the total Voronoi volume for that particle.

a function of ϕ , shown in Fig. 5. In [27], this phenomena is observed, but the density is apparently independent of the volume fraction, and occurs at the same value of n for each packing. For packings approaching RCP, the extensive nature of the fluctuations occurs at $n_c \approx 100$, lower than $n_c \approx 1000$ for RLP. Figure 6 shows the fluctuation density, $\langle (\mathcal{W}_n - \langle \mathcal{W}_n \rangle)^2 \rangle_n = \frac{\langle (\mathcal{W}_n - \langle \mathcal{W}_n \rangle)^2 \rangle}{n}$, or fluctuation per grain, as a function of ϕ for all packings used herein

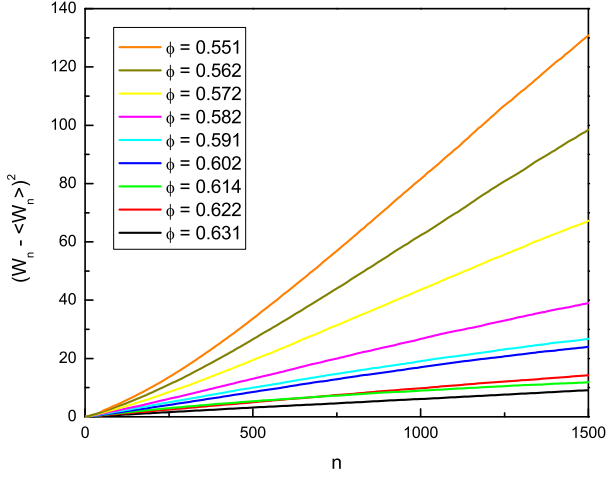


FIG. 4: $\langle \Delta \mathcal{W}_n^2 \rangle_n$ versus n_c for packings with $\mu \rightarrow \infty$, with $Z \approx 4.3$, for different ϕ .

obtained for $n > n_c$. This data represents the main equation of state for all of the numerical packings considered herein. Each color curve represents packings with a fixed Z (or μ) as indicated in the figure. We note that while the fluctuations for all $Z(\mu)$ in this study collapse onto a single curve, as illustrated in Fig 6, the limit of integration, $\phi_{\text{RLP}}(Z)$ in Eq. (9), changes as discussed in the phase diagram of [8], increasing as μ decreases and effectively depending on Z as $\phi_{\text{RLP}}(Z)$. Indeed, $\phi_{\text{RLP}}(Z)$ is the theoretical RLP line depicted as a dashed line in Fig. 2. These equations of state should be compared with an analogous equation of state obtained in [26] for jammed packings equilibrated using a fluidized bed. The fluctuations presented in Fig. 6 monotonically decrease as ϕ increases, and do not display a parabolic shape as depicted in [26]. While the protocol used herein, the "split" algorithm presented in Section II.A [8], and the protocol for the experiments of [26] differ, we would expect that the equation of state should be the same. Elucidation regarding this difference requires further investigation.

An important note is that this extensive relationship occurs well before n is large enough such that finite size effects of the system force the fluctuations to tend to zero. Further, the linear relationship extracted from n -clusters is different from that extracted from n randomly chosen Voronoi cells, implying a correlation between Voronoi cell volumes, revealed using the clustering technique. Analysis of the fluctuation density reveals the following formula

$$\begin{aligned} \Delta \sigma_n^2 &\equiv \langle (\mathcal{W}_n - \langle \mathcal{W}_n \rangle)^2 \rangle_n = \frac{1}{2} ((\sigma_{n+1}^2 - \sigma_n^2) + (\sigma_n^2 - \sigma_{n-1}^2)) \\ &= \sigma_1^2 + \langle \mathcal{W}_n \Delta \mathcal{W}_{n+1} \rangle + \langle \mathcal{W}_{n-1} \Delta \mathcal{W}_n \rangle \\ &\quad - \langle \mathcal{W}_n \rangle \langle \Delta \mathcal{W}_{n+1} \rangle - \langle \mathcal{W}_{n-1} \rangle \langle \Delta \mathcal{W}_n \rangle, \end{aligned} \quad (6)$$

where σ_1^2 is the single particle, or microscopic, fluctuation in Voronoi volume, and $\Delta \mathcal{W}_{n+1} = \mathcal{W}_{n+1}^{\text{vor}} - \langle \mathcal{W}^{\text{vor}} \rangle$ is the $n+1$ free Voronoi volume to be added to the clus-

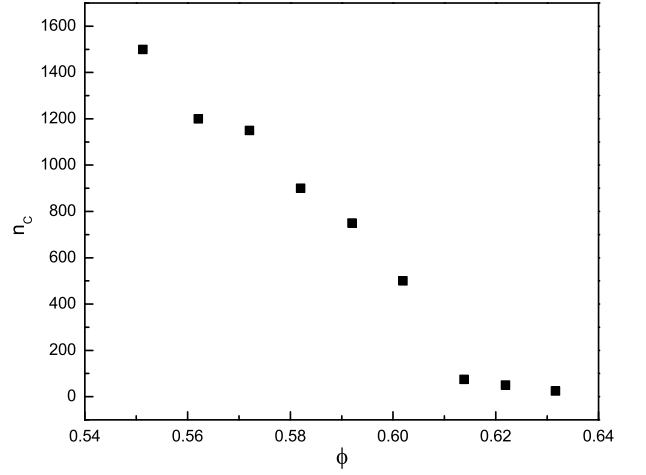


FIG. 5: n_c vs ϕ showing maximal value of extensive nature. Values of ϕ are taken along $\mu \rightarrow \infty$, with $Z \approx 4.3$, to display largest range of ϕ .

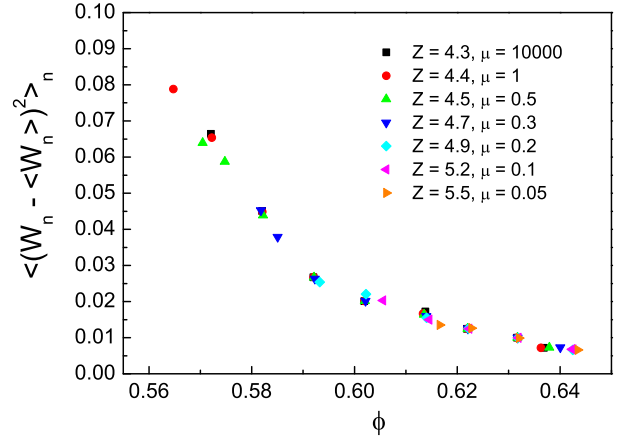


FIG. 6: $\langle \Delta \mathcal{W}_n^2 \rangle_n$ versus ϕ for packings with different friction coefficients producing different mechanical coordination number versus the volume fraction. Each dataset with fixed coordination number corresponds to the packings along each horizontal line in Fig. 2.

ter of n free Voronoi volumes being averaged. If volumes are chosen randomly, as opposed to the clustering condition, the fluctuation density collapses to the microscopic fluctuation density, σ_1^2 , as the correlation tends to zero. Therefore, the fluctuations will scale exactly with n , as indicated in [27]. Further, if the averaging process is taken to be equal to or larger than the system size, then $\langle \Delta \mathcal{W}_{n+1} \rangle = \langle \Delta \mathcal{W}_n \rangle = 0$, such that Eq. (6) is rewritten as

$$\Delta \sigma_n^2 = \sigma_1^2 + \langle \mathcal{W}_n \Delta \mathcal{W}_{n+1} \rangle + \langle \mathcal{W}_{n-1} \Delta \mathcal{W}_n \rangle. \quad (7)$$

Equation (7) thereby provides an analytical form for the curves presented in Fig. 4, as a function of n . Future work may take into consideration n th neighbor coordination and distance distribution, as in [28].

Compactivity.—The compactivity is then obtained via the integration of Eq. (5):

$$X^{-1} = \lambda \int_{\phi(X)}^{\phi_{\text{RLP}}(Z)} \frac{d\langle \mathcal{W}_n \rangle}{\langle (\mathcal{W}_n - \langle \mathcal{W}_n \rangle)^2 \rangle}, \quad (8)$$

where we use that $\phi(X \rightarrow \infty) \rightarrow \phi_{\text{RLP}}$ [8]. Since Voronoi volumes are additive, $\langle \mathcal{W}_n \rangle = \langle \mathcal{W} \rangle = NV_g/\phi$. The fluctuations in Voronoi volume are divided by the number of grains, N , thereby introducing the fluctuation density, shown in Fig. 6 into Eq. (8). Therefore, the above integration is rewritten as:

$$(X/V_g)^{-1} = \lambda \int_{\phi_{\text{RLP}}(Z)}^{\phi(X)} \frac{d\phi}{\phi^2 \langle (\mathcal{W}_n - \langle \mathcal{W}_n \rangle)^2 \rangle_n}, \quad (9)$$

and we may then utilize the fluctuations as a function of ϕ , and integrate along a line of constant $Z(\mu)$. The assumption that $\sigma_n^2(V)/\langle V \rangle^2 = \sigma_n^2(\phi)/\langle \phi \rangle^2$ is not utilized here, as done in [26], explaining the different functional form for the compactivity of Eq. (9) from that of [26].

Following the above presented method, $\phi_{\text{RLP}}(Z)$ is extracted from the phase diagram, and used as a limit of integration in order to calculate $X(\phi)$ from fluctuations in Voronoi volume, in Eq. (9). This introduces the dependence on Z as $\phi(X)$ is obtained by integrating Eq. (9) numerically by applying a fitting function to the numerical data of Fig. 6. The equation of state, $\phi(X)$ for a given Z , is plotted in Fig. 7 for different values of the average coordination number of the packings, $Z(\mu)$, revealing that as we approach $\phi_{\text{RCP}} \approx 0.645$, $X \rightarrow 0$, regardless of the value of μ . Further, $X \rightarrow \infty$ as we approach ϕ_{RLP} , with the smallest volume fraction of the RLP appearing for $\mu \rightarrow \infty$ and $Z \approx 4$ in the high-compactivity limit, $\phi_{\text{RLP}} \approx 0.55$. The compactivity curve plotted in Fig. 7 is continuous, even though the volume fluctuation data is the result of a discrete set of simulations as seen in Fig. 6. This is due to the fact that we smoothly interpolate a continuous curve for the volume fluctuations as a function of ϕ , resulting in a smooth integration for the compactivity, and subsequently the entropy through Eq. (9).

Entropy.—The entropy, S , and its density, $s = S/N$, are obtained by integrating

$$X^{-1} = \frac{\partial S}{\partial V}. \quad (10)$$

By virtue of having a fixed total volume, V , for any particular system defined by ϕ , we can substitute $V = NV_g/\phi$ such that:

$$(X/V_g)^{-1} = -\phi^2 \frac{\partial s}{\partial \phi} \quad (11)$$

Using the concept that ϕ_{RCP} is a fixed value in the phase diagram for all values of $Z(\mu)$, we integrate between the limits of ϕ_{RCP} and the desired ϕ .

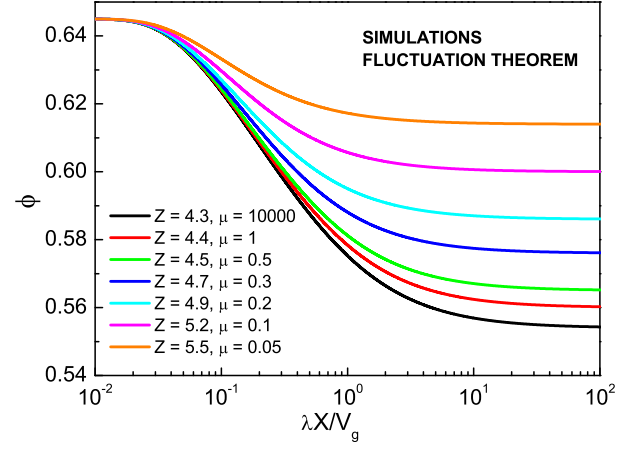


FIG. 7: ϕ versus X from the integration of Voronoi volume fluctuations. The smoothness of the curves is due to the fact that we use fitting functions for the data in Fig. 6 to perform the integration of Eq. (9)

$$s(\phi) - s(\phi_{\text{RCP}}) = \lambda \int_{\phi}^{\phi_{\text{RCP}}} \frac{d\phi}{(\lambda X/V_g)\phi^2}. \quad (12)$$

Equations (9) and (12) can be combined to provide an equation for s as a function of the Voronoi volume fluctuations.

$$s(\phi) = \lambda \int_{\phi}^{\phi_{\text{RCP}}} \frac{d\phi'}{\phi'^2} \int_{\phi_{\text{RLP}}(Z)}^{\phi'} \frac{d\phi''}{\phi''^2 \langle (\mathcal{W}_n - \langle \mathcal{W}_n \rangle)^2 \rangle} + s(\phi_{\text{RCP}}). \quad (13)$$

Therefore, we can calculate $s(\phi)/\lambda$, based on the fluctuations of a packing of jammed grains for a fixed Z , following the horizontal lines in Fig. 2. Integration of the compactivity curve achieved via simulation provides the entropy, up to a constant value at ϕ_{RCP} , as defined by Eq. (12). The entropy of the packings from simulations in Fig. 2 is plotted in Fig. 8 as a function of ϕ for different values of Z . The shape of the entropy curve is in qualitative agreement with that calculated by Aste and collaborators using X-ray tomography techniques to determine the position of particles inside large scale packings, as shown in [29].

D. Entropy from Information Theory

Analysis of the entropy from fluctuations in Voronoi volume clusters provides a value for entropy density up to a constant of integration $s(\phi_{\text{RCP}})$, as shown in Eq. (13). To obtain the entropy of RCP we use an independent method based on information theory as developed in [30, 31], related to the thermodynamic entropy in [32], and applied to emulsion systems in [33] which does not require a constant of integration. This method provides a second

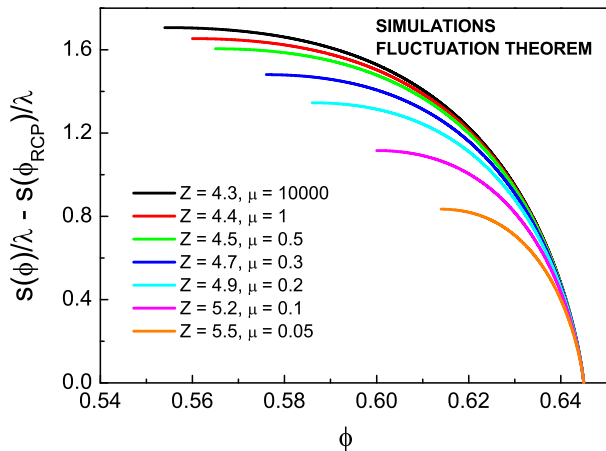


FIG. 8: Entropy density versus ϕ from the integration of X.

estimate of the entropy for all volume fractions to be compared with Fluctuation theory.

We use the Voronoi cell and Delaunay triangulation for each particle to define a Voronoi network by considering contacts when a Voronoi side is shared between two particles, and hence are Delaunay contacts, as shown in Fig 3. In order to facilitate periodic boundary conditions, we surround the finite box enclosing all Voronoi cells with 26 virtual boxes. These boxes enclose virtual particles, translated in all possible combinations from the real box. QHull calculates all Delaunay contacts, and only those pairs of contacts which contain at least one real particle are considered, while pairs of virtual contacts are discarded, thus ensuring complete periodic boundary conditions.

A graph is constructed as a cluster of n particles that are Delaunay contacts, and by means of graph automorphism [34] can be transformed into a standard form or "class" i of topologically equivalent graphs that are considered a state with a probability of occurrence p_i . Reference [34] provides the code to deal with isomorphic graphs, which is essential for counting different graph classes. The topological equivalence accounts for graphs with varied Voronoi cell sizes and locations while retaining identical lists of consecutive subsets of Delaunay contacts. In practice, we determine p_i by extracting a large number m of clusters of size n from the system and count the number of times, f_i , a cluster i is observed, such that:

$$p_i = f_i/m. \quad (14)$$

A simple example of graph classes can be seen when $n = 3$. Figure 9 shows exactly 4 possible graphs that can be achieved, consisting of 0, 1, 2 and 3 connections between 3 Delaunay contacts. Each graph falls into a class of $i = 0 \rightarrow 3$. The random process of selecting a graph with $n = 3$ is done m times, continuously calculating the probability of f_i , as defined in Eq. (14).

The Shannon entropy of a clusters of size n is thereby defined as:

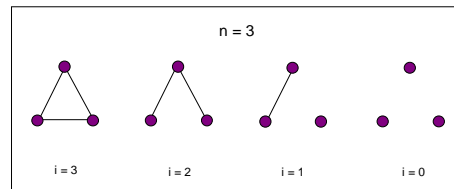


FIG. 9: Classes of graphs for $n=3$. There are only 4 possible graphs, 0 contacts, 1 contact, 2 contacts, or 3 contacts.

$$H(n) = -\lambda \sum p_i \ln p_i. \quad (15)$$

Equation (15) reduces to the thermodynamic entropy if one replaces the probability, p_i , with the Boltzmann factor. The name Shannon entropy does not imply that Eq. (15) is a new kind of entropy. It merely implies that we will calculate the entropy of the packing using information theory methods, which is routinely applied to sequences.

Ideally, m is large enough such that the values of p_i converge to a fixed value for each value of n , such that the Shannon entropy converges as well. Computationally, for large n , it is not possible to reach this convergence within a reasonable time, and certain approximations can be applied as outlined in [35] to decrease the number of iterations necessary, summarized briefly here.

As one iteratively selects clusters, increasing m by one each time, new classes of graph are obtained, such that we have a total number of different graphs k , where $k \leq m$. While Fig. 9 depicts the relatively simple case of $n = 3$, higher values of n have a significantly larger number of graph classes. Therefore, Eq. (14) is only an approximation of the true probability of observing a cluster i and can be rewritten as

$$p_i \approx f_i/m, \quad (16)$$

where the equation becomes an equality as $m \rightarrow \infty$. We must therefore replace Eq. (15) by

$$H^*(n) = -\lambda \sum \frac{f_i}{m} \ln \frac{f_i}{m}. \quad (17)$$

Graphs with f_i/m smaller than $1/m$ will likely be observed only once, if at all. This finite-size effect grows with increasing n , as graphs become very complex. The quantity $H_1(n)$ is defined as the contribution to $H^*(n)$ of the topologies observed once. Measurements where $H_1(n)$ exceeds a threshold percentage of $H^*(n)$ are not considered to be valid measurements.

In an effort to improve convergence, and thereby decrease simulation time for the calculation of the configurational entropy, a finite sample correction is applied. The details of this correction are presented herein, as well as in [35].

Referring now to H^* from above, the probability $P_i(f_i)$ that a certain state i will be observed exactly f_i times is given by the binomial distribution

$$P_i(f_i) = \binom{m}{f_i} p_i^{f_i} (1 - p_i)^{m - f_i}. \quad (18)$$

Define the probability of a certain event to be p_i , the number of observed events to be m and the number of uniquely observed events to be k . Furthermore let $F(x)$ be a function that can be Taylor expanded around p_i :

$$F(x) = F(p_i) + F'(p_i)(x - p_i) + \frac{1}{2}F''(p_i)(x - p_i)^2 + \dots \quad (19)$$

The binomial distribution is concentrated around the average $\langle f_i/m \rangle = p_i$, and we obtain the following useful approximation using the definition of the variance in a binomial distribution:

$$\begin{aligned} \langle F(\frac{f_i}{m}) \rangle &= F(p_i) + F'(p_i)\langle \frac{f_i}{m} - p_i \rangle + \frac{1}{2}F''(p_i)\langle (\frac{f_i}{m} - p_i)^2 \rangle + \dots \\ &= F(p_i) + \frac{1}{2}F''(p_i)\frac{p_i(1 - p_i)}{m} + \dots \end{aligned} \quad (20)$$

Let $F(x) = -x \log x$, an obvious choice considering the form of the Shannon entropy. Then, $F''(x) = -1/x$ and

$$\langle F(\frac{f_i}{m}) \rangle = -p_i \log p_i - \frac{1 - p_i}{2m}, \quad (21)$$

Therefore,

$$\begin{aligned} \frac{\langle H^* \rangle}{\lambda} &= \sum_i \langle F(\frac{f_i}{m}) \rangle = - \sum_i p_i \log p_i - \frac{\sum_i (1 - p_i)}{2m} + \dots \\ &= \frac{H}{\lambda} - \frac{k - 1}{2m} + \dots, \end{aligned} \quad (22)$$

The Shannon entropy is then the calculated entropy from the average of H^* obtained from multiple simulations, plus the binomial correction term $(k - 1)/2m$, since the sum over all p_i is unity, a term clearly tending to zero as m tends to infinity. This approximation works well under two conditions. First, $mp \geq 1$, in order to allow the Taylor expansion to converge. Second the contribution of the probabilities below $1/m$ to the Shannon entropy must be a practically insignificant term. If this is not the case, additional binomial correction terms must be used. However, these terms will not be independent of p_i , therefore making the calculation significantly more complicated. It is of interest in the present work to ensure that both conditions necessary for the use of only the first term of the binomial correction are applicable.

Assuming the above described binomial distribution of the probability of having a cluster of class i observed exactly f_i times, the first order finite sampling correction to H^* therefore results in

$$\frac{H(n)}{\lambda} = \frac{H^*(n)}{\lambda} + \frac{k - 1}{2m}. \quad (23)$$

The entropy must be further corrected to account for the Shannon entropy as measured for a crystal structure by using the methods presented herein. The entropy of a crystal structure where $N \rightarrow \infty$ should be zero, and as such an FCC packing should have zero entropy. However, when applying the graph counting method explained above to a finite system, a crystal structure will present a non-zero entropy. It is important to subtract the entropy of a finite crystal structure from the Shannon calculations. In studies of network forming materials outlined by [31], an empirical correction term of $g(n) = (d - 1) \log(n)$ is subtracted from each value of $H(n)$, where d is the dimensionality of the network. The functional form of $g(n)$ is obtained by applying the above described Shannon entropy calculation directly to an FCC packing, and its results are shown in Fig. 10. During the process of randomly selecting m points in the network, some points will inevitably fall inside of the grain boundaries. Points approaching the center of a grain will have a different set of n nearest grain centers than points chosen outside of the grain boundary. This discrepancy is accounted for via $g(n)$. In the present study, this term is augmented by using the exact values obtained for $g(n)$, and not the empirical form, as shown in Fig 10. It should be noted that the empirical form for $g(n)$ comes very close to the exact values, differing only by an approximately exact constant. For calculations of entropy density, differences between successive values of $H(n)$ result in the cancellation of this constant, exemplified below.

We redefine the Shannon entropy as follows:

$$\frac{H'(n)}{\lambda} = \frac{H(n)}{\lambda} - g(n), \quad (24)$$

and the entropy density is

$$s = \lim_{n \rightarrow \infty} [H'(n + 1) - H'(n)] \quad (25)$$

Figure 11 shows the calculation of $H'(n)$ versus n for a typical packing with $\mu = 10000$ and $\phi = 0.64$. We show that $s(n)$ converges so rapidly, as shown in Fig. 11 such that even moderate values of n ($n \geq 8$) are enough to obtain a sufficient approximation of s [31]. The calculation is repeated for all the packings and the Shannon entropy density is plotted in Fig. 12 versus ϕ for different $Z(\mu)$.

When examining values of the Shannon entropy for values of $\phi < \phi_{RCP}$, Fig. 12 displays an increase in the entropy as volume fraction decreases, similar to that of the entropy as calculated via Voronoi volume fluctuation density in Fig 8. However, this increase does

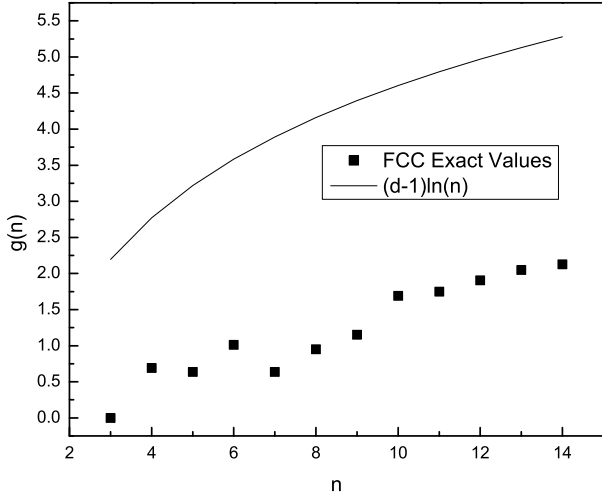


FIG. 10: Entropy of crystal (FCC) packing as calculated using graph theoretical methods. While the entropy is approximately equal to $(d-1)\ln(n)$, minus a meaningless constant, exact values from simulations are used herein.

not appear dependent on the mechanical coordination number of the packings. Further, the Shannon entropy does not increase by the same magnitude as observed in the entropy from fluctuations. For instance, from the fluctuation theorem calculations of Fig. 8 we find $s_{\text{RLP}} - s_{\text{RCP}} = 1.7\lambda$ while from the Shannon entropy of Fig 12 we find $s_{\text{RLP}} - s_{\text{RCP}} = 0.35\lambda$. As suggested in [35], this discrepancy may be due to the additional entropy arising from freedom to move grains within the packing without disrupting the Delaunay network, and hence not affecting the probabilities in Eq. (16). Analysis of such volume contributions to the Shannon entropy requires a Monte Carlo simulation, in which the available phase space volume that the packings can explore for a fixed graph is probed [35], with the additional constraint that the packing must maintain the Delaunay contact network under all possible rearrangements. This calculation is considered in [35] and will be the topic of future study.

Figure 12 shows that as we approach ϕ_{RCP} for all values of Z using information theory, $s/\lambda \simeq 1.1$. We therefore define $s(\phi_{\text{RCP}})/\lambda = 1.1$, the value of the entropy as calculated via graph theoretical methods.

Thus, the Shannon entropy density provides an estimation of the entropy for the RCP state, $s(\phi_{\text{RCP}}) \approx 1.1\lambda$, serving as the constant of integration for the entropy density as realized by Fluctuations Theorem. Under this approximation, we can shift the Fluctuation Theorem entropy of Fig. 8 vertically by $s_{\text{RCP}} = 1.1\lambda$ as calculated via Shannon entropy methods. Figure 13 shows the entropy shifted by this constant value, as calculated via simulation. It is important to emphasize that $s(\phi_{\text{RCP}})$ is approximate, due to neglecting fluctuations of the fixed Delaunay network as explained above. Nevertheless, we remark that the obtained value of s_{RCP} is compatible

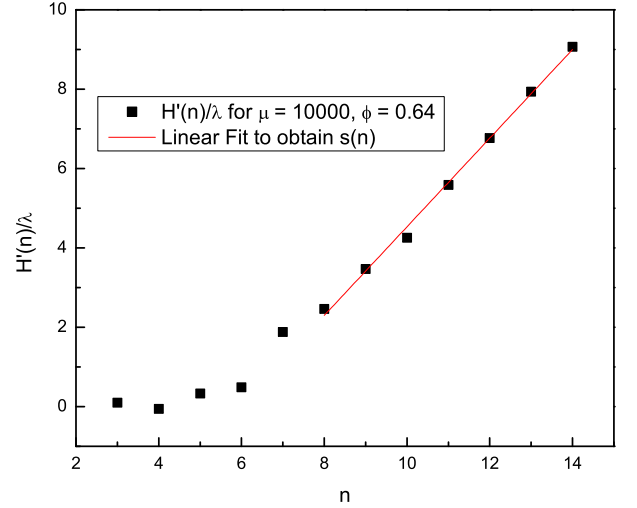


FIG. 11: Shannon entropy function of n , with $\mu = 10000$ and $\phi = 0.64$. The red line displays a linear fit between $n = 8$ and $n = 14$, from which the entropy density is extracted. This process is repeated for all packings used herein.

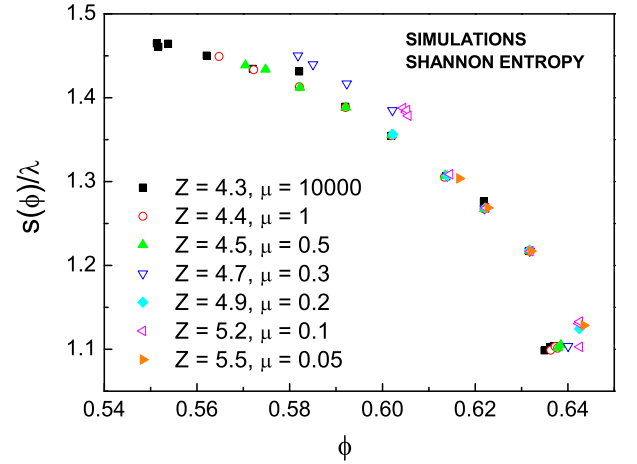


FIG. 12: Shannon entropy density, $s(\phi)$ for all packings used herein. The minimum value of the entropy density is achieved at RCP, and is used as a constant of integration for the entropy obtained from Fluctuation theorem.

with other estimates which found the entropy of the order λ (see for instance the calculation of the analogous complexity, Σ , by Zamponi and Parisi who found $\Sigma/\lambda \sim 1$ [36]).

III. THEORETICAL MODEL

In this section we develop a theoretical framework to understand the numerical results in light of [8].

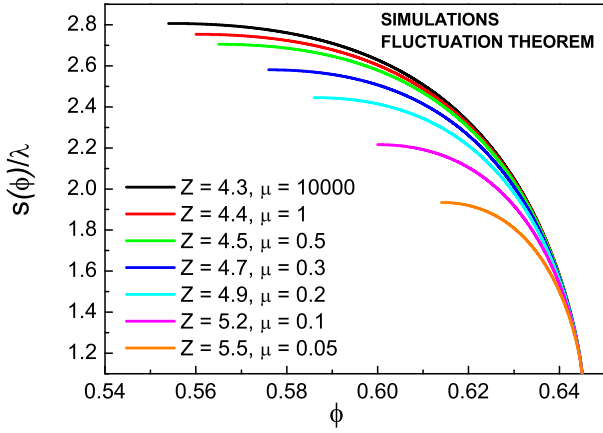


FIG. 13: Entropy at RCP achieves a value of 1.1 as calculated by the Shannon Entropy at RCP and serves as a constant of integration for the entropy from Fluctuation theorem in Fig. (8) producing the entropy shown in this figure.

A. Statistical mechanics of frictional hard spheres

Experiments of shaken grains, fluidized beds and oscillatory compression of grains [25, 26, 27, 37, 38] indicate that granular materials show reversible behavior, and the analogue of the conserved energy, E , in thermal systems is the volume $V = NV_g/\phi$, for a system with N grains of volume V_g at position \vec{r}_i . Thus, the number of configurations, Ω , and the entropy in the micro-canonical ensemble of jammed hard spheres is defined as [14]:

$$\Omega(V) = e^{S(V)/\lambda} = \int \delta(V - \mathcal{W}(\vec{r}_i)) \Theta_{\text{jam}}(\vec{r}_i) \mathcal{D}\vec{r}_i. \quad (26)$$

Analogous to the temperature in equilibrium system $\partial E/\partial S = T$, the “temperature” in granular matter is the compactivity, $X = \partial V/\partial S$. Here $\Theta_{\text{jam}}(\vec{r}_i)$ is a constraint function restricting the integral to the ensemble of jammed states, $\mathcal{W}(\vec{r}_i)$ is the volume function associated with each particle taking the role of the Hamiltonian in thermal systems which is defined in terms of the Voronoi volume in Eq. (4). The crux of the matter is then to properly define Θ_{jam} and \mathcal{W} to calculate the entropy and volume in the ensemble of jammed matter.

Volume ensemble.— A minimum requirement of $\Theta_{\text{jam}}(\vec{r}_i)$ is to ensure touching grains, and obedience to Newton’s force and torque laws. As in the numerical simulations, the volume function, $\mathcal{W}(\vec{r}_i)$, is taken as the volume of the Voronoi cell associated with each particle at position \vec{r}_i , for which the analytical form has been obtained in Eq. (4) [8]. The entropy in the V-ensemble of

frictional hard spheres is:

$$e^{S(V)/\lambda} = \int \delta(V - \mathcal{W}(\vec{r}_i)) \times \prod_i \left\{ \delta\left(\sum_{j \neq i} \vec{f}_{ij}\right) \delta\left(\sum_{j \neq i} \vec{f}_{ij} \times \vec{r}_{ij}\right) \delta(\vec{f}_{ij} - \vec{f}_{ji}) \times \prod_{j \neq i} \left[\Theta(\mu f_{ij}^N - f_{ij}^T) \delta\left([\vec{r}_{ij}^2 - 1\right](\vec{f}_{ij}^2) \mathcal{D}\vec{f}_{ij} \right] \mathcal{D}\vec{r}_i \right\}, \quad (27)$$

where $\vec{r}_{ij} \equiv \vec{r}_i - \vec{r}_j$, the normal inter-particle force is $f_{ij}^N \equiv |\vec{f}_{ij} \cdot \hat{r}_{ij}|$, the tangential force: $f_{ij}^T \equiv |\vec{f}_{ij} - (\vec{f}_{ij} \cdot \hat{r}_{ij})\hat{r}_{ij}|$. All quantities are assumed properly dimensional for simplicity of notation. The terms inside the brackets $\{\cdot\}$ correspond to the jamming constraint function Θ_{jam} in Eq. (26), and therefore define the ensemble of jammed states. The first three δ -functions inside the big brackets impose Newton’s second and third law. The Heaviside Θ -function imposes the Coulomb condition and the last δ -function the touching grain condition for hard spheres, assuming identical grains of unit radius. Integration is over all forces and positions which are assumed to be equally probable as in the flat average assumption in the micro-canonical ensemble.

An extra term should be added as $\delta\left(\frac{1}{2N} \sum_{i \neq j} (\vec{f}_{ij} \otimes \vec{r}_{ij}) - \bar{\sigma}\right)$ where, for the isotropic case, the stress tensor is $\sigma_{\alpha\beta} = p\delta_{\alpha\beta}$, with p the pressure. Since we are treating hard spheres, the pressure p just controls the mean value of forces and does not contribute to the statistics. Thus, this term is not needed, which means that the angoricity, $A = \partial p/\partial S$, is irrelevant for hard spheres. At the isostatic limit $p \rightarrow 0$, and further assuming a Boltzmann distribution of pressure [39, 40, 41, 42, 43], similar to that of mesoscopic volumes [8], such a term would tend towards unity in a partition function for jammed matter. However, the angoricity should be considered in the case of deformable grains, a system of future studies.

Clearly, Eq. (27) is almost intractable from an analytical point of view. However, under the quasi-particle approximation of [8] we can define the configurational entropy at the mesoscopic level using a corollary of the force-balance ensemble: the isostatic conjecture and a coarse-grain volume function in terms of the coordination number as we show in Section III.B.

It is of interest to determine if the ensemble defined by Eq. (27) satisfy the definition of jamming given by Torquato [12]. A definition of jammed configurations based on force/torque balance is a necessary condition for mechanical equilibrium of a packing with friction and frictionless grains. A force-balanced packing is defined as the existence of a set of forces $\{\vec{f}_{ij}, \forall \text{ balls } i \text{ in contact with ball } \alpha\}$ such that the sum of the forces/torques for each particle is zero,

$$\sum_j \vec{f}_{ij} = 0, \quad \sum_j \vec{f}_{ij} \wedge \hat{n}_{ij} = 0, \quad (28)$$

with the non trivial contact forces $\sum_{ij} |\vec{f}_{ij}| = 1$, $\vec{f}_{ij} \cdot \hat{n}_{ij} \geq 0$ where \hat{n}_{ij} is the unit vector of the contact j . Other necessary mechanical constraints should be added too, e.g. $\vec{f}_{ij} \wedge \hat{n}_{ij} = 0$ for frictionless packings.

While the above conditions are necessary for jamming they are not sufficient. To define a more restricted force-balance condition we consider that the contacts around a ball i are *not degenerated* if \exists a neighbor α such that

$$\vec{f}_{i\alpha} \cdot \hat{k} \neq 0, \quad \forall \hat{k} \neq 0. \quad (29)$$

This condition assures that at least one contact force is off-plane. A packing is *restrict force-balanced* if it is force-balanced and the contacts around all the balls are not degenerated.

A question is raised whether the restrict force-balance condition for the frictionless case fits the geometrical definition of Torquato [12]. It can be proved that packings with (28) and (29) are at least locally jammed. To see this, let us formalized the locally jammed condition as follows: for any ball i , there is at least one contact $\hat{n}_{i\alpha}$ such that $\hat{n}_{i\alpha} \cdot \hat{k} > 0$, $\forall \hat{k} \neq 0$. Since the contact force $\vec{f}_{i\alpha}$ is parallel with $\hat{n}_{i\alpha}$ for frictionless packings, the condition is equal to $\vec{f}_{i\alpha} \cdot \hat{k} < 0$. From the non-degenerated condition, there must be a contact satisfying $\vec{f}_{i\alpha} \cdot \hat{k} \neq 0$. Assuming $\vec{f}_{i\alpha} \cdot \hat{k} > 0$ (otherwise we prove the result directly), there must exist another contact α' that $\vec{f}_{i\alpha'} \cdot \hat{k} < 0$ because of the force-balance condition, then $\sum_j \vec{f}_{ij} \cdot \hat{k} = 0$.

Thus we prove a sufficient condition for local jammed configuration from the force balance point of view. Accordingly, the non-degenerated condition is necessary for the proof above. Since it not necessary it could also satisfy more stringent geometrical definitions, e.g. collective jammed, or even strict jammed, but this has to be figured out in further investigation. Although the restrict force-balance condition is not always satisfied in our simulations, the bias is very small. In frictionless packings it implies that the coordination number must be larger than d ; a small fraction of particles with $Z < d$ are found in simulated packings as well as experimental ones. By removing the degenerated balls recurrently (for instance it is a common practice to remove floaters), we end up with a packing satisfying the constraint of non-degeneracy and therefore being locally jammed. Thus we expect that many experimental packings satisfy the restrict force-balance condition. The force-balance condition can be extended to the frictional cases, by simply adding the constraint between normal and tangential forces. Finally, the ensemble in Eq. (27) is assumed to satisfy the restrict force-balance condition. Thus, it is understood that the condition of Eq. (29) is implicit in the ensemble average of Eq. (27).

Assuming that the conditions specified in Eq. (27) are met in the numerical packings, the simulation results can be interpreted as the ensemble average Eq. (27). However, there is a further important distinction between Eq. (27) and the numerical calculations. Equation (27) assures that all configurations at a given volume have the

same probability. This is the flat average assumption in the micro-canonical ensemble that allows for the development of statistical mechanics. Without this assumption statistical calculations are impossible to perform (see however [44] for a thorough discussion). There is no rigorous proof that the flat average assumption is correct in equilibrium statistical mechanics. Still, its validity is widely accepted. For granular matter, use of the flat average is much more controversial. Earlier simulations [38] indicate some evidence for ergodicity. The ergodic hypothesis implies not only the equal probability of states but also that for sufficiently long times the phase trajectory of a closed system passes arbitrarily close to a manifold defined by a constant volume (or energy) [45]. Experiments indicate reversible behavior, supporting that the flat average can be applied to granular matter, although this assertion is certainly not true in general.

We notice that Eq. (27) is difficult to solve. Analytical progress can be done by considering a coarse-graining of the Voronoi volume function and working with quasiparticle theory developed in [8] to obtain a configurational entropy at the mesoscopic level.

B. Volume Function

The mesoscopic theory presented in [8] and [23] coarse grains the Voronoi volumes of a jammed granular packing over a mesoscopic length scale and calculate an average volume function. The coarsening reduces the degrees of freedom to one variable, the geometrical coordination number of each grain, z , that allows for an analytical solution of the partition function. We find a mesoscopic free volume function [8]:

$$w(z) \equiv \frac{\langle \mathcal{W}_i^{vor} \rangle - V_g}{V_g} = \frac{2\sqrt{3}}{z}, \quad (30)$$

Here, we note that \mathcal{W}_i^{vor} has been rigorously defined in Eq. (4), validated its equivalence to the Voronoi volume, and its use in comparison between simulation results and a statistical mechanics formulation utilizing the Voronoi cell as the microscopic volume associated with each grain.

If the system is fully random we can extend the assumption of uniformity from the mesoscopic scale to the macroscopic scale, such that we arrive to an equation of state relating $\phi^{-1} = w + 1$ with z as:

$$\phi = \frac{z}{z + 2\sqrt{3}}. \quad (31)$$

C. Partition Function

Below, we briefly discuss the results of [8] regarding the phase diagram.

We assume that the sum over each quasiparticle with volume $w(z)$ is the total volume [23], then the canonical partition function for a single particle can be written as:

$$\mathcal{Z}_{\text{iso}} = \int g(z) e^{-\frac{w(z)}{\lambda X}} dz \quad (32)$$

Equation (32) is the single particle partition function, such that the full partition function for N particles is $\mathcal{Z}_{\text{iso}}^N/N!$.

The density of states, $g(z)$ is assumed to be analogous to the result when the discreteness of phase space imposed by the Heisenberg uncertainty principle in quantum mechanics. We assume the density of states to be only a function of the geometrical coordination number, as the volume function from Eq. (30) reduces the degrees of freedom for jammed granular matter to z . The density of states is thereby conjectured to take the form [8]:

$$g(z) = (h_z)^{z-2d}, \quad (33)$$

where h_z is the analogue of the Planck constant (see [8] for more details).

The most populated state is the highest volume at $z = 4$ while the least populated state is the ground state at $z = 6$. This assumed form of Eq. (33) is an approximation, and will be further addressed below. Since the term $1/(h_z)^{2d}$ is a constant, it will not influence the average of the observables in the partition function, although it changes the value of the entropy by a constant independent of ϕ .

Conditions of isostaticity provide the lower bounds of the geometrical coordination number as $Z \leq z$, while considering disordered states and hard sphere conditions imposes $z \leq 6 \leq 2d$. which induce bounds upon the limits of integration in the partition function, and account for the jamming restriction, Θ_{jam} . Here, Z is the mechanical coordination number related to the force balance (that is, counting the contacts with non-zero forces) while z is the geometrical coordination number related to the geometry of the contact network. Z ranges between $Z = d + 1$, for infinite friction grains, and $Z = 2d$, for frictionless grains as given by the isostatic conjecture discussed by Alexander [15] and in many subsequent papers. Further detail on this notion is available in [8].

Substituting Eq. (30) and Eq. (33) and the isostatic condition into Eq. (32), we find the isostatic partition function:

$$\mathcal{Z}_{\text{iso}}(X, Z) = \int_Z^6 (h_z)^{z-2d} \exp\left(-\frac{2\sqrt{3}}{zX}\right) dz. \quad (34)$$

Obtaining the phase diagram is then a matter of calculating the average volume fraction, $\phi(X, Z)$ by solving the partition function for different values of X and Z .

$$\phi(X, Z) = \frac{1}{\mathcal{Z}_{\text{iso}}(X, Z)} \int_Z^6 \frac{z}{z + 2\sqrt{3}} \exp\left(-\frac{2\sqrt{3}}{zX} + z \ln h_z\right) dz. \quad (35)$$

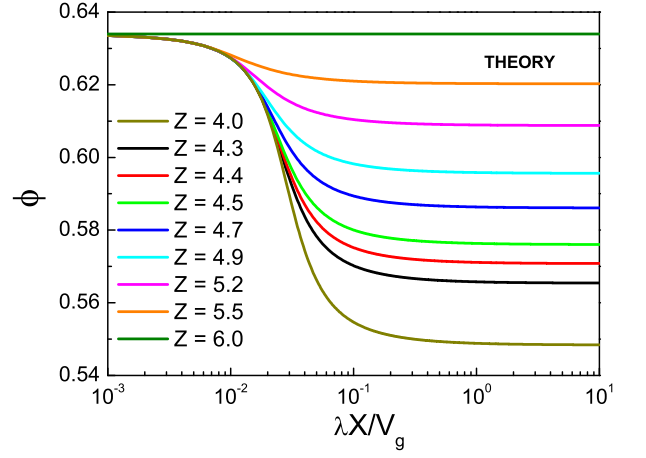


FIG. 14: Prediction of the mesoscopic theory for $\phi(X)$.

The boundaries of the phase diagram are plotted in Fig. 2 along with the packings obtained via simulation. We note that Z_{RCP} from simulations appears slightly higher than $Z = 6$, falling closer to $Z_{\text{RCP}} = 6.2$ as shown in Fig. 2. We will use this value as $Z_{\text{max}} = 6.2$ when considering it in the partition function as an upper bound for the jamming condition in an effort to accurately analyze the simulation results and characterize the entropy. Further, since the variation in Z is small as we examine lines of constant μ , the average of $Z(\mu)$ can be used as the lower bound of the limit in the partition function.

D. Compactivity

The results presented in Fig. 7 are compared to the theoretical model presented above. The theoretical calculation for $\phi(X)$ is achieved exactly as described for $\phi(Z)$ in Eq. (35), and is presented in Fig. 14.

In the limit of vanishing compactivity ($X \rightarrow 0$) for the theoretical model, only the minimum volume or ground state at $z = 6$ contributes to the partition function. Then we obtain the RCP state, $\phi_{\text{RCP}} = \phi(X = 0, Z) = \frac{6}{6+2\sqrt{3}} \approx 0.634$, for all values of Z . In the limit of infinite compactivity ($X \rightarrow \infty$), the Boltzmann factor $e^{-\frac{2\sqrt{3}}{zX}} \rightarrow 1$, and the average in (35) is taken over all the states with equal probability. Assuming $h_z \ll 1$, the leading contribution to the average value is from the highest volume at $z = Z$ and therefore we obtain

$$\phi_{\text{RLP}}(Z) \approx \frac{Z}{Z + 2\sqrt{3}}. \quad (36)$$

The dotted line in Fig. 2 is a plot of the equation of state presented in Eq. (36). It is an important result that the values of $\phi_{\text{RLP}}(Z)$ well fit $\phi = \frac{Z}{Z+2\sqrt{3}}$. On the other hand, there are states to the right of the RCP line in Fig. 2. These states are a manifestation of the microscopic fluctuations, and not taken into account by the present mesoscopic theory.

The general shape of $\phi(X)$, achieved via simulation well matches that as predicted by the mesoscopic theory, if not in magnitude, when using an exponential form for $g(z)$. The compactivity achieves maximal value at the minimal available volume fraction, as observed both when examining the fluctuations in Voronoi volume and within the confines of the mesoscopic theory. Packings near RLP, being the least dense, have the greatest room to be further compacted, or increase density, and therefore approach infinite compactivity. Packings near RCP, being the most dense, have either minimal or zero room for to be further compacted, and therefore cannot increase density and tend towards zero compactivity. This helps to establish the concept of compactivity as a static "effective temperature", acting as a state variable that may link the results of packings preparation and specific packing protocols to the statistical mechanics formulation. Indeed, these results for $\phi(X)$ qualitatively resemble the compaction curves obtained in the experiments of [25]. We also note that the results of Fig. 14 are qualitatively similar to a simple mean-field two state model predicted by Edwards, where RCP and RLP are obtained in the limits of $X \rightarrow 0$ and $X \rightarrow \infty$, respectively [14].

E. Entropy

Comparison to the theoretical model proceeds by defining the equation of state for the entropy density. The entropy density is obtained as:

$$s_{\text{meso}}(X, Z) = \langle w \rangle / X + \lambda \ln \mathcal{Z}_{\text{iso}}(X, Z) \quad (37)$$

This equation is obtained in analogy with equilibrium statistical mechanics and it is analogous to the definition of free energy: $F = E - TS$ where $F = -k_B T \ln \mathcal{Z}$ is the free energy. We replace $k_B T \rightarrow \lambda X$, $E \rightarrow \langle w \rangle$. Therefore, $F = E - TS$ or $S = (E - F)/T = E/T + \ln \mathcal{Z}$ is now $s(X, Z) = \langle w \rangle / X + \lambda \ln \mathcal{Z}_{\text{iso}}(X, Z)$. The partition function is evaluated by a numerical integration of Eq. (34) for a fixed Z and as a function of X . A numerical interpretation of Eq. (35) then provides ϕ versus X for a fixed Z , a result that is plotted in Fig. 14. Using these two results the entropy is obtained using Eq. (37). Values of the theoretical entropy density are plotted in Fig. 15 for several values of Z . By fixing Z , we are equivalently imposing a fixed μ upon the system, as $Z(\mu)$ is determined by μ exclusively within the confines of this model.

We see that the theoretical entropy density captures the general behavior found in the simulations as shown in Fig. 13, i.e., it is maximal as we approach RLP for $Z = 4$ and $X \rightarrow \infty$ while approaching the minimum entropy at RCP. Furthermore, all the curves for different Z approach $S \sim \ln X$ as $X \rightarrow 0$, similar to a thermal ideal gas. At the mesoscopic level, the entropy vanishes at RCP. In fact it diverges to $-\infty$ when $\phi \rightarrow \phi_{\text{RCP}}$ closer

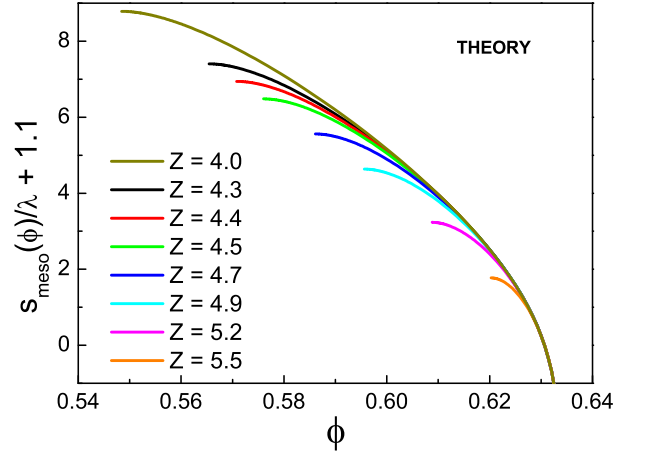


FIG. 15: Prediction of the mesoscopic theory for $s_{\text{meso}}(\phi)$.

than a constant proportional to h_z (once again assuming an exponential distribution for $g(z)$), much like the Planck constant imposes a finite size in the phase space of quantum mechanics. Thus, we assert that the value of ϕ at which $s(\phi) = 0$ in the theoretical model provides a definition of RCP at the mesoscopic level. The theoretical $\phi(X)$ arising from Fig. 14 is also in qualitative agreement with the simulation results of Fig. 7.

We use $h_z = 0.01$ in Fig. 15 such that the mesoscopic entropy vanishes very close to the predicted value of $\phi_{\text{RCP}} \approx 0.634$ [8]. However, the maximum value of $\phi_{\text{RCP}} \approx 0.642$ from simulation, introduces a discrepancy between the theoretical and simulated models.

The value of h_z is chosen to fit the mesoscopic theory of Fig. 15 with simulation as close as possible, where the only constraint imposed by theory is $h_z < 1$. While the values of both ϕ_{RCP} and $\phi_{\text{RLP}}(Z)$ from the theory are well reproduced by the simulation results, it is clear that the values of s are not, as evidenced by comparing Fig. 15 with Fig. 13. For example, from simulations we find $s_{\text{RLP}} = 2.8\lambda$ at $Z = 4.3$ and theory predicts $s_{\text{RLP}} = 8.8\lambda$. This is directly due to the magnitude of h_z , and its implications towards the density of states, $g(z)$. If we examine $s(X \rightarrow \infty, Z)$, we achieve the entropy as a function of Z along the RLP line. When $X \rightarrow \infty$, the equation of state in Eq. (37) is rewritten as

$$s_{\text{meso}}(X \rightarrow \infty, Z) = \lambda \ln \int_Z^{Z_{\text{max}}} (h_z)^z dz, \quad (38)$$

where $Z_{\text{max}} = 6.2$. This equation is exactly solvable, resulting in the following formula for the mesoscopic entropy along the RLP line.

$$s_{\text{meso}}(X \rightarrow \infty, Z) = \lambda \ln \left(\frac{h_z^{Z_{\text{max}}} - h_z^Z}{\ln h_z} \right). \quad (39)$$

Adjusting the value of h_z directly affects the mesoscopic entropy along the RLP as defined by Eq. (39). A

similar analysis has been used to obtain the functional form for $\phi(X \rightarrow \infty, Z)$ along the RLP line.

$$\phi(X \rightarrow \infty, Z) = \frac{\ln h_z}{h_z^{Z_{max}} - h_z^Z} \int_Z^{Z_{max}} \frac{z}{z + 2\sqrt{3}} (h_z)^z dz. \quad (40)$$

Equation (40) is the equation of state for the RLP line, and is plotted in Fig. 2 in the limit $h_z \rightarrow 0$ when it reduces to Eq. (36). However, for a general h_z , Eq. (40) applies. While this equation is not exactly solvable, it is easily seen that changing h_z will not only impact the magnitude of the mesoscopic entropy along the RLP line of Eq. (39), but also impact the values of $\phi_{RLP}(Z)$ which define the left most boundary of the phase diagram. Further, the effect on one will be the inverse of the effect on the other. Simply stated, within the present mesoscopic framework, one cannot satisfy fitting both the value of the entropy at, for instance, RLP and the value of ϕ_{RLP} in the phase diagram from simulation to the mesoscopic theory where h_z is the only adjustable parameter.

F. Mesoscopic and Microscopic Fluctuations

Near RCP the mesoscopic entropy vanishes. More specifically, it diverges to $-\infty$ when $\phi \rightarrow \phi_{RCP}$ closer than a constant proportional to h_z , providing a characterization of RCP at the mesoscopic level. This result qualitatively resembles behavior of the complexity of the jammed state in the replica approach to jamming [30, 31]. We identify this point as a mesoscopic “Kauzmann point”, in analogy with the density, or temperature, at which the configurational entropy of a colloidal, or molecular, glass vanishes at the ideal glass transition [46]. From this point the entropy increases monotonically with X , being maximum for the RLP limit. An important result is the direct implication of a larger number of states available to jammed systems at RLP with respect to any higher volume fraction, directly implying maximal entropy at the RLP limit. Packings with packing fractions above RCP to $\phi_{FCC} = 0.74$, the optimal packing fraction for spheres in 3d, do not appear in our theory because they exhibit some degree of order, or crystallization. By doing so, we explicitly do not consider crystals or partially crystalline packings in the ensemble. This is a direct consequence of setting the upper limit: $z \leq 6$. States with $\phi > \phi_{RCP}$ are new microscopic states of the system, and their existence requires further theoretical investigation.

At RCP, we find minimal fluctuation with respect to Voronoi volumes associated to each grain. This implies the surprising conclusion of a minimal number of mesoscopic states for frictionless systems at RCP. Considering these minimal fluctuations to be essentially zero, RCP has zero entropy and no fluctuations with respect to a mesoscopic coarse-graining over the ensemble. This is the frictionless jamming transition [4, 5] or J-point

[4, 5, 7]. We see that, in principle, at the mesoscopic level this transition point is well-defined. However a mesoscopic state parameterized by a given average coordination number contains many microscopic states which are averaged out in the coarse-graining procedure to calculate the volume function at the quasi-particle level. For instance, while the isostatic condition requires $Z = 2d$ contacts per grain averaged over the entire packing, it makes no implication towards the exact distribution of contacts per individual grain. This allows for the existence of microscopic states with grains having $Z < 2d$ and $Z > 2d$ within the packing. Therefore we expect that these microscopic states contribute to a nonzero entropy at the J-point at RCP. Indeed the Shannon entropy calculation of Section II.D finds the entropy of RCP to be $s_{RCP} = 1.1\lambda$.

The full entropy should consider both mesoscopic and microscopic contributions, such that

$$s = s_{meso} + s_{micro}. \quad (41)$$

The mesoscopic contribution is obtained via the theory, while the microscopic contribution can be obtained herein using the Shannon entropy method. We know that $s_{RCP} = 1.1\lambda$ from simulations and $s_{meso} = 0$ from theory. Therefore, the total entropy at RCP is just the microscopic entropy, $s_{RCP} = s_{micro}(RCP)$, which is equal to 1.1λ from simulations. Thus, $s_{micro}(RCP) = 1.1\lambda$. This result is understood since all the jammed states are degenerate around the mesoscopic ground state with the coordination number $z = 6$. As noted, these states still have slightly different volume fractions, which leads to the microscopic fluctuations which are coarse-grained in the mesoscopic theory. At the present time we do not have a theory to explain the value of 1.1λ since the mesoscopic theory does not include microscopic states nor fluctuation in the coordination number. Next, we make the additional assumption that the microscopic entropy is independent of the volume fraction and can therefore consider $s_{micro}(\phi) = s_{micro}(RCP) = 1.1\lambda$ for all values of ϕ between RCP and RLP. The result is the total entropy of the packing as

$$s(\phi) = s_{meso}(\phi) + 1.1\lambda \quad (42)$$

for any ϕ , where s_{meso} is calculated by Eq. (37). Equation (42) is plotted in Fig. 15. Where the mesoscopic entropy is augmented by its fixed value at RCP, and this value is $s_{RCP} = 1.1\lambda$. We reiterate that in Fig. 15, the addition of 1.1 to $s_{meso}(\phi)$ makes two assumptions. First, it assumes that $s_{meso}(RCP) = 0$ as predicted by theory. Second, it assumes that $s_{micro}(\phi) = s_{micro}(RCP) = 1.1\lambda$, as determined by the Shannon entropy method, and is not an explicit function of ϕ .

The mesoscopic entropy is $s_{meso} = 0$ not only at RCP but for $\phi_{RCP} \leq \phi \leq \phi_{FCC}$. This implies an intrinsic difference between the current theory and Edwards’ statistics given by Eq. (27) leading to the separation of the entropy in terms of the different length scales as in Eq. (41).

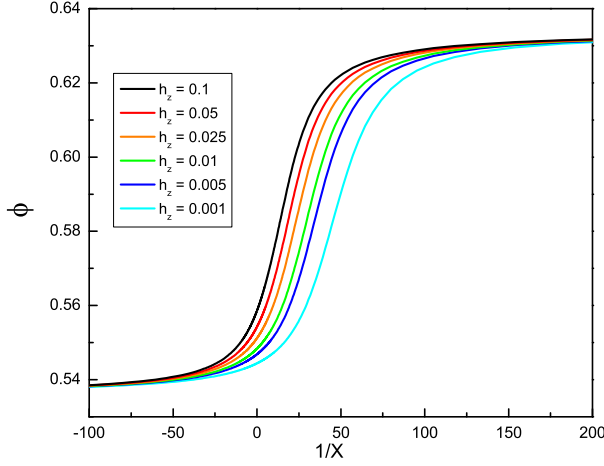


FIG. 16: Volume fraction as a function of the inverse of compactivity, for $Z = 4$, as calculated using theoretical methods, including negative compactivity values, for h_z ranging from 0.001 to 0.1. When X discontinuously jumps from ∞ to $-\infty$, $\phi(X)$ exhibits continuous behavior. However, when X continuously goes from 0^- to 0^+ , $\phi(X)$ exhibits a discontinuous jump from ≈ 0.536 to ≈ 0.634 .

G. Negative Compactivity

Analyzing the partition function from a mathematical approach, we are interested in the concept of negative compactivity and its effect on the equation of state.

When $X \rightarrow 0^+$, $\phi(X \rightarrow 0^+) \rightarrow \phi_{RCP}$. Under the assumption of a very large $g(z)$ at $z = Z$, with respect to any higher z , $X \rightarrow +\infty$, $\phi(X \rightarrow +\infty) \rightarrow \phi_{RLP}(Z) = \frac{Z}{Z+2\sqrt{3}}$, where Z is the lower limit of integration in Eq. (35). This occurs because when using the density of states of Eq. (33), with $h_z \rightarrow 0$, $g(z) \sim \delta(z - Z)$. However, as evidenced above, an exponential form for $g(z)$ may not well reproduce simulation results for the entropy. Altering $g(z)$ is shown to better reproduce the entropy equation of state, but shifts the predicted value of ϕ_{RLP} higher. Examination of a negative compactivity within the above presented statistical mechanics framework should allow us to achieve the minimum value of RLP in the limit $X \rightarrow 0^-$. For a background on negative temperature states in equilibrium statistical mechanics see Landau and Lifshitz book on statistical physics. Note that a negative temperature state is "hotter" than a state at absolute zero temperature and any positive temperature state. The state with $T \rightarrow +\infty$ is physically identical to the state with $T \rightarrow -\infty$. As in magnetic systems where negative temperature states can be observed, granular matter is characterized by a bounded volume fraction and "thermalization" of volume at a negative temperature is possible, in principle. Next, we analyze those states with a negative compactivity.

When $X \rightarrow 0^+$, the Boltzmann factor in the partition function of Eq. (34) tends towards zero. As such, the largest value of z , or the smallest value of $1/z$ will

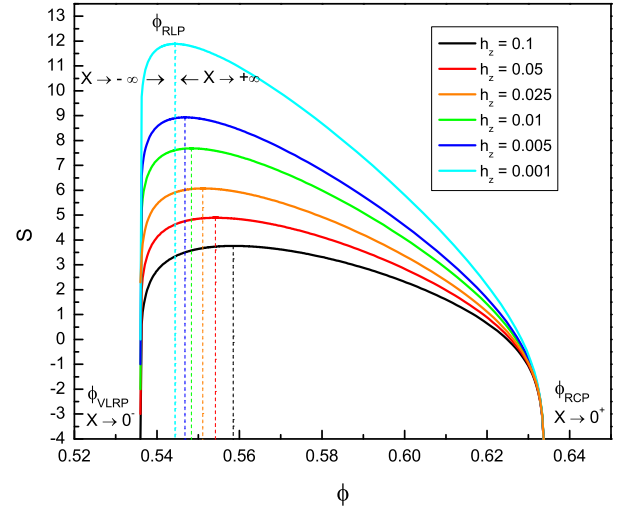


FIG. 17: Entropy plotted for $Z = 4$, as calculated using theoretical methods, including negative compactivity values. $S(\phi)$ tends towards $-\infty$ at $\phi = 0.536$ ($X \rightarrow 0^-$) and $\phi = 0.634$ ($X \rightarrow 0^+$), the minimal value of RLP and RCP, respectively, for any value of h_z . Dashed vertical lines show $\phi(X)$ for $X \rightarrow \pm\infty$, acknowledging the lowest physically achievable volume fraction at $Z = 4$ for a particular value of h_z . Larger values of h_z result in larger values of $\phi(X \rightarrow \pm\infty)$. Following [20] we call $\phi(X \rightarrow 0^-) \rightarrow \phi_{VLRP}$ (very loose random packing), $\phi(X \rightarrow \pm\infty) \rightarrow \phi_{RLP}$ and $\phi(X \rightarrow 0^+) \rightarrow \phi_{RCP}$. In the limit of $h_z \rightarrow 0$ the difference between VLRP and RLP vanishes $\Rightarrow \phi_{VLRP}^{h_z \rightarrow 0} \rightarrow \phi_{RLP}$. The maximum entropy is always at RLP. Negative compactivity states are very difficult to obtain with current protocols.

give the largest value of the Boltzmann factor when using the partition function to calculate observable averages. This results in the calculation of the RCP state. However, when $X \rightarrow 0^-$, the Boltzmann factor in the partition function tends towards infinity, not zero, and the largest value of Z , or the smallest value of $1/z$ will give the largest value of the Boltzmann factor. When calculating the average volume function in either case, the density of states will not greatly impact the results with respect to the contribution from the Boltzmann factor. Therefore, when $X \rightarrow 0^-$, the average volume fraction will reduce to the predicted value of the RLP line where $h_z \rightarrow 0$, $\phi(X \rightarrow 0^-, Z) = \phi_{RLP}(Z) = \frac{Z}{Z+2\sqrt{3}}$. Figure 16 exemplifies this phenomenon, plotting $\phi(X)$ at $Z = 4$ for different values of h_z .

The entropy equation of state should achieve the same values as $X \rightarrow +\infty$ and $X \rightarrow -\infty$, since the Boltzmann factor approaches unity in either case. Although not as obvious, the same can be said for $X \rightarrow 0^+$ and $X \rightarrow 0^-$. The equation of state (37) can be rewritten as:

$$s_{\text{meso}}(X, Z)/\lambda = \ln \int_Z^6 (h_z)^{z-2d} e^{-\frac{1}{\lambda X}(w(z) - \langle w(z) \rangle)} dz. \quad (43)$$

In the case of $X \rightarrow 0^+$, X is positive, and $w(z) \geq$

$\langle w(z) \rangle$, as RCP represents the lowest attainable value of $\langle w(z) \rangle$. The exponentiated term in the partition function is always negative, such that the entropy approaches $-\infty$. Conversely, when $X \rightarrow 0^-$, X is negative, and $w(z) \leq \langle w(z) \rangle$, and we obtain the highest attainable value of $\langle w(z) \rangle$. Again, the exponentiated term in the partition function is always negative, such that the entropy approaches $-\infty$.

Figure 17 displays the equation of state for $Z = 4$ as calculated by the theoretical model of Eq. (43). We use $Z = 4$ and $Z_{max} = 6$ as the limits of integration for the partition function of Eq. (34). The value of h_z is increased to show that larger values of $g(z)$ at RLP result in a more precise agreement between $\phi(X \rightarrow \pm\infty)$ and $\phi(X \rightarrow 0^-)$. The dashed vertical lines of Fig. 17 show $\phi(X)$ for $X \rightarrow \pm\infty$, acknowledging the lowest physically achievable volume fraction at $Z = 4$ for a particular value of h_z . Larger values of h_z result in larger values of $\phi(X \rightarrow \pm\infty)$, allowing for the existence of a greater range of packings with a negative compactivity, having $\phi(X \rightarrow 0^-) < \phi < \phi(X \rightarrow -\infty)$.

Some models exist where the concept of a negative temperature finds physical meaning, including nuclear spins and semiconducting lasers. In Ref. [20] an attempt is made to include the concept of a negative temperature within a statistical mechanics framework. By means of a lattice model in $2d$, utilizing a discrete phase space, mechanically stable packings, or microstates, are shown to exist beneath the volume fraction with the largest number of microstates, at a particular μ . The highest entropy occurs when the largest number of microstates are available, and is the equivalent of ϕ_{RLP} in the above presented mesoscopic theory. Under the assumption of an ergodic exploration of the volume fractions available to the lattice model, this implies that packings with $\phi < \phi_{RLP}$ exist, with entropy below the maximal value, and that these packings can be explained via the concept of a negative temperature. Reference [20] thereby considers ϕ_{RLP} to be the "loosest possible random packing that is mechanically stable that one can achieve by pouring grains". Below this limit there exists RVLP "random very loose packings" with negative temperature.

Although the present work analyzes packings in $3d$, the results of mesoscopic theory find agreement with the simulations of [20]. The main results of [8], Fig. 2 and for instance Eq. (36) have been obtained in the limit of $h_z \rightarrow 0$. If we relax this constraint then negative compactivity states are possible. We assert that these states exist because there is an upper bound in the volume function at $z = Z$. Systems with unbounded volume functions (Hamiltonians) do not allow for negative compactivity (temperature) states. In this context we have the definition of the following limits according to the entropy and compactivity: The RCP limit is $\phi(X \rightarrow 0^+) = \phi_{RCP}$ and minimum entropy: Neglecting the negative diverging of the entropy we have $S_{RCP} = S(X \rightarrow 0^+) \rightarrow 0$. The RLP limit is defined as the maximum entropy in the limit $\phi(X \rightarrow \pm\infty) = \phi_{RLP}$. If h_z is finite then

VLRP appears as $\phi(X \rightarrow 0^-) = \phi_{VLRP}$ and minimum entropy. Again, neglecting the divergency, we obtain $S_{VLRP} = S(X \rightarrow 0^-) \rightarrow 0$. In the limit of $h_z \rightarrow 0$ the difference between RLP and VLRP vanishes and we have only one well defined RLP as: $\phi_{RLP}^{h_z \rightarrow 0} \rightarrow \phi_{VLRP}$.

Fig. 17 shows a maximal entropy at ϕ_{RLP} , indicating the largest number of available microstates to the system. The introduction of a negative compactivity, as described above, allows the theory to probe states such that $\phi < \phi_{RLP}$. It becomes apparent that the range of ϕ in which these states may exist is directly related to the magnitude of h_z , decreasing as the discretization of phase space within the confines of the mesoscopic theory such that in the limit of a continuous phase space none of these packings are mechanically stable. Our theoretical model includes the concept of a discrete phase space for jammed grains, and our simulations show that $h_z < 1$, but not necessarily $h_z \ll 1$. Further, the "split" algorithm utilized simulates a pouring of grains with respect to the method of packing creation. It is possible that the concept of a negative compactivity could help to explain areas in the phase diagram of Fig. 2 unavailable within the scope of the present study.

IV. OUTLOOK

Although extensive detail is presented in this study regarding the various steps necessary to analyze the equations of state, several questions remain unclear.

(a) The derivation of the entropy for jammed granular matter is explicitly calculated via fluctuations in Voronoi cell volume for each packing presented herein. As we are studying random packings, crystal states are not achieved with anything other than measure zero probability. Thus, the highest available volume fraction for any given packing is RCP, $\phi \simeq 0.64$, not FCC, $\phi = 0.74$, as corroborated by simulation results. This result is the apparent limit of the preparation protocols used herein. It can be said with certainty that a FCC packing has zero fluctuation with respect to their constituent Voronoi cells. At RCP simulations reveal a non-zero fluctuation, as discussed above. This approach, however, does not account for the possibility that for packings above RCP, but below FCC, may achieve a continuous, monotonic, degree of crystallization. Such a condition would permit a continuous decrease in fluctuation to exactly zero, from RCP to FCC, which can be studied within the scope of a more complete theory that includes random and partially crystallized packings.

Below we elaborate on a possible scenario to rationalize the transition from disorder at RCP to order at FCC. If the microscopic fluctuations are not subtracted from RCP then the compactivity curves presented in Fig. 7 no longer reach a plateau when approaching RCP, but reach a finite, non-zero, value. This opens the possibility that a true thermodynamic phase transition may occur at RCP between a disordered phase and an ordered phase.

It remains possible that a phase transition occurs at RCP, and packings of higher volume fraction need not preserve the properties of a fully random system. It remains an open topic how one would define compactivity between RCP and FCC, as compactivity has been herein attributed to packing protocols resulting in random packings.

The mesoscopic theory of [8] utilized herein considers a vanishing entropy at, or near, RCP. Taking into consideration the FCC state, a more complete theory including packings between RCP and FCC should be characterized, such that the entropy of jammed matter approaches zero when approaching FCC, not RCP. Furthermore, the result that $X \rightarrow 0$ at RCP is merely an artifact of the mesoscopic theory that neglects microscopic fluctuations. A full theory would obtain $X \rightarrow 0$ at FCC. Figure 18 displays a possible interpretation for an extension of the entropic equation of state. The entropy attains a maximal value at ϕ_{RLP} , as predicted by the existing mesoscopic theory. When $\phi_{RLP} < \phi < \phi_{RCP}$, the packing consists of purely random states, and the entropy decreases as we approach RCP from lower volume fractions, also as predicted. At some point close to ϕ_{RCP} , the entropy deviates from its predicted decrease to zero at ϕ_{RLP} , and follows a different branch. When $\phi_{RCP} < \phi < \phi_{FCC}$ a coexistence between random and crystalized microstates may exist, ultimately leading to a purely crystalized packing at FCC. The exact nature of the transition, continuous or discontinuous, from purely random states to a coexistence of states remains an open topic. The incorporation of microscopic fluctuations and microscopic crystalized states into the existing mesoscopic theory may result in a more complete characterization of the entropy of jammed granular matter, a work currently in progress.

(b) An additional assumption made in calculating the compactivity of jammed granular matter is that those packings along the RLP line have $X = \infty$. This assumption directly allows for the $\phi(X)$ equation of state without any constants due to integration techniques. It appears to be reasonable to presume that X is large along the simulated RLP line, with respect to X of all other packings used herein, and that the constant term $\frac{1}{X(\phi_{RLP})}$ is very small.

(c) As mentioned above, there exists a small fluctuation density in Voronoi volume at RCP. The fluctuation density increases as we increase n , and comes to a maximal value at a particular range of n , where n is larger as we approach lower values of ϕ as shown in Fig. 5. This increase in value is due to selecting of clusters of n Voronoi volumes, as opposed to n randomly chosen grains. In the case of randomly chosen grains, the fluctuation density remains constant, equal to the fluctuation at $n = 1$. Such a change implies a correlation between the Voronoi volumes in clusters of grains, exemplified by Eq. (7). This correlation may create a scale separation, such that microscopic correlations dominate the fluctuations at lower n and mesoscopic correlations dominate at higher n . This scale separation would result in a difference between local and global compactivities, suggested

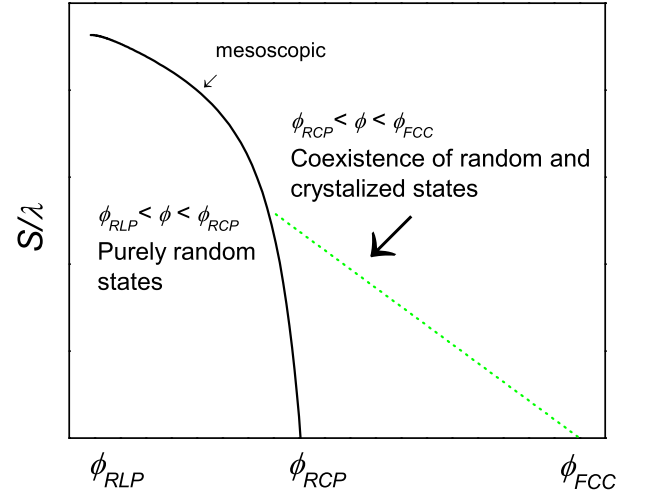


FIG. 18: A possible extension of the entropy equation of state to include packings between RCP and FCC. For $\phi_{RLP} < \phi < \phi_{RCP}$, the packing consists of only random states, and the entropy decreases when approaching RCP from lower volume fractions, as predicted by the mesoscopic curve. At ϕ_{RCP} , the entropy does not decrease to zero, as predicted by the mesoscopic curve, and follows a different branch, achieving exactly zero entropy at ϕ_{FCC} . When $\phi_{RCP} < \phi < \phi_{FCC}$ a coexistence between random and crystalized microstates may exist. The possible existence of a transition that may define RCP remains an open question.

in [47], and is a topic of continuing study. It also remains possible that fluctuation densities calculated using larger n sized clusters overuse the data set by largely repeating constituent Voronoi cells in cluster volumes, thereby rendering the fluctuation densities questionable for packings approaching RLP. Again, it should be noted that simply using the microscopic fluctuations does not greatly effect the entropy calculations.

(d) The mesoscopic theory predicts $S \rightarrow -\infty$ as we approach RCP for any μ . This concept does not adhere to physical measurements, where the minimal entropy should be zero. Taking this into consideration, another method must be used to calculate the entropy of packings at RCP, independent of the distribution of Voronoi volumes used to facilitate the mesoscopic theory. The Shannon entropy calculation applies graph theoretical methods, resulting in a non-zero value for the entropy of RCP, well suited for a more complete equation of state. While it can be said with some degree of certainty that the Shannon entropy calculation contributes to the entropy at RCP, it is unclear whether it does so completely. Other methods may be available that provide all of the entropy at RCP, or give additional terms to the Shannon entropy, another topic of continuing study. Further, as discussed above with respect to fluctuation density, packings between RCP and FCC have partial degrees of crystallization, such that the entropy of an FCC is exactly zero, or $-\infty$ as described in the theory. Recent work [29] suggests that the entropy experiences an increase immediately fol-

lowing RCP, due to mixing between random and crystal states. Incorporation of these ideas into the present work remains a topic of ongoing study.

(e) While the concept of negative compactivity works well as a mathematical tool for achieved the VLRP state of jammed granular matter, it remains difficult to attribute a physical meaning to such a condition. Recent studies in [20] suggest that negative compactivity probes mechanically stable states that exist beneath RLP, but are not accessible by means of grain pouring. It should be noted that $X < 0$ states may not be thermalized with $X > 0$. Such ideas will remain the topic of future studies.

(f) An exponential density of states with a very small value of h_z provides a very accurate phase diagram, in comparison with simulations, but values for the entropy that are different by a factor of 4 times larger than those achieved via simulation. It remains possible that the methods presented herein simply do not capture all of the entropy for jammed matter, and larger values from simulation are possible, such that corrections to the mesoscopic theory could be minimized. Further, a new theory that carefully analyzes all packings up from ϕ_{RLP} through $\phi_{\text{FCC}} = 0.74$ may result in the ability to capture all of the entropy for a given packing. Current work is approaching this idea from a microscopic level.

(g) The differences displayed between theoretical and simulated entropy can to some extent be considered within the scope of disagreement between classical and quantum entropy. Classical entropy measurements are primarily interested in ΔS , having a minimum value of 0 when approaching the ground state, though $S \rightarrow -\infty$. Quantum entropy measurements assume a minimum value of phase space over which one can integrate degrees of freedom for a give system. This results in a $S = 0$ exactly at the ground state. Determination of a well defined minimum phase space volume for jammed matter would adjust the number of available microstates, Ω , within the micro-canonical ensemble as presented by Edwards. Such a model may be available through a careful analysis of the microscopic entropy, including partially crystalized states above ϕ_{RCP} through the crystal state of ϕ_{FCC} , the highest achievable packing fraction for identical spheres in $3d$.

V. CONCLUSIONS

Simulation results as derived from mesoscopic fluctuations are presented in Figs. 7 and 8. When comparing all the packings with different $Z(\mu)$ and ϕ , the maximum entropy is at the minimum volume fraction of RLP ϕ_{RLP} when $X \rightarrow \infty$ but only infinite friction. The minimum entropy is found for the RCP state at ϕ_{RCP} for $X \rightarrow 0$, now for all the values of friction, indicating the degener-

acy of the RCP state. It is commonly believed that the RCP limit corresponds to a state with the highest number of configurations and therefore the highest entropy. This belief is expressed for instance in the definition of RCP as the maximally random jammed state [12]. However, here we show that the states with a higher compactivity have a higher entropy, corresponding to the looser RLP packings. Within a statistical mechanics framework of jammed matter, this result is a natural consequence, and gives support to such an underlying statistical picture.

Each curve in the Figs. 14 and 15 correspond to a system with a different $Z(\mu)$, as calculated using a mesoscopic ensemble. When comparing all the packings, the maximum entropy is at ϕ_{RLP} and $X \rightarrow \infty$ while the entropy is minimum for ϕ_{RCP} at $X \rightarrow 0^+$. Following the $Z = 4$ line in the phase diagram we obtain the entropy for infinitely rough spheres showing a larger entropy for the RLP than the RCP. The same conclusion is obtained for the other packings at finite friction ($4 < Z(\mu) < 6$). We conclude that the RLP states are more disordered than the RCP states. Approaching the frictionless J -point, $\mu \rightarrow 0$ ($Z = 6$) the entropy vanishes. More precisely, it vanishes for a slightly smaller ϕ than ϕ_{RCP} of the order h_z . Strictly speaking it diverges to $-\infty$ at ϕ_{RCP} as $S \rightarrow \ln X$ for any value of Z , in analogy with the classical equation of state. However, this is an unphysical limit, as it would be considering distances in phase space smaller than the minimal distance in the jamming phase space. Thus we consider only packings with an entropy density greater than or equal to 0 as "physical" packings. We note that the compactivity curves from the theoretical model match simulation with accuracy. The theoretical entropy fails to agree with the entropy from simulation in magnitude, but reproduces the overall shape. While increasing h_z such that the magnitude of the entropy from the mesoscopic theory would decrease, the RLP line would no longer be well reproduced. As simulations and theory are in strong agreement with respect to the RLP line, increasing h_z does not appear to be a reasonable amendment to the mesoscopic partition function.

In summary, a notion of disorder is presented that applies to frictional hard spheres, as well as frictionless ones. The entropy reveals interesting features of the RCP and RLP states such as the fact that RLP is maximally random with respect to RCP and that both limits can be defined in terms of the entropy and equation of state. Overall, the agreement between theory and simulation is sufficient to indicate that the methods presented herein are appropriate for evaluating the entropy of jammed matter.

Acknowledgements. - We express our thanks for the financial support of NSF and DOE. We further thank Kun Wang and Yuliang Jin for insightful discussions.

[1] S. F. Edwards and D. V. Grinev, in *Jamming and Rheology*, Eds. A. Liu and S. R. Nagel (Taylor and Francis,

New York, 2001).

- [2] A. Coniglio, A. Fiero, H. J. Herrmann and M. Nicodemi eds. *Unifying Concepts in Granular Media and Glasses* (Elsevier, Amsterdam, 2004).
- [3] A. J. Liu and S. R. Nagel, *Nature* **396**, 21 (1998).
- [4] H. A. Makse, D. L. Johnson, and L. M. Schwartz, *Phys. Rev. Lett.* **84**, 4160 (2000);
- [5] H. Zhang and H. A. Makse, *Phys. Rev. E* **72** 011301 (2005).
- [6] R. C. Ball and R. Blumenfeld, *Phys. Rev. Lett.* **88**, 115505 (2002).
- [7] C. S. O'Hern, S. A. Langer, A. J. Liu, S. R. Nagel, *Phys. Rev. Lett.* **88**, 075507 (2002).
- [8] C. Song, P. Wang, H. A. Makse, *Nature* **453**, 629 (2008):arXiv:0808.2196.
- [9] Onoda, G. Y. & Liniger, E. G. *Phys. Rev. Lett.* **64**, 2727-2730 (1990).
- [10] J. D. Bernal, *Nature* **185**, 68 (1960).
- [11] S. Torquato, T. M. Truskett, and P. G. Debenedetti, *Phys. Rev. Lett.* **84**, 2064 (2000).
- [12] S. Torquato and F. H. Stillinger, *J. Phys. Chem B* **105**, 11849 (2001).
- [13] T. Under, J. Kertesz, and D. E. Wolf, *Phys. Rev. Lett.* **94**, 178001 (2005)
- [14] S. F. Edwards and R. B. S. Oakeshott, *Physics A* **157** 1080 (1989).
- [15] S. Alexander, *Phys. Rep.* **296**, 65 (1998).
- [16] L. E. Silbert, *et al.* *Phys. Rev. E* **65**, 031304 (2002).
- [17] Stealing the gold: a celebration of the pioneering physics of Sam Edwards, P. M. Goldbart, N. Goldenfeld, D. Sherrington, eds. (Oxford Science Publications, Oxford, 2004).
- [18] C. F. Moukarzel, *Phys. Rev. Lett* **81**, 1634 (1998)
- [19] W.G. Ellenbroek, E. Somfai, M. van Hecke, and W. van Saarloos, *Phys. Rev. Lett.* **97**, 258001 (2006).
- [20] M. P. Ciamarra and A. Coniglio, *Phys. Rev. Lett.* **101**, 128001 (2008).
- [21] L. D. Landau and E. M. Lifshitz, *Theory of Elasticity*, (Pergamon, NY, 1970).
- [22] R. D. Mindlin, *J. Appl. Mech. (ASME)* **71**, (1949).
- [23] C. Song, P. Wang, H. A. Makse: arXiv:0808.2186.
- [24] T.C. Hales, The Kepler Conjecture, <http://arxiv.org/abs/math.mg/9811078>
- [25] E. R. Nowak, J. B. Knight, E. BenNaim, H. M. Jaeger and S. R. Nagel, *Phys. Rev. E* **57**, 1971 (1998).
- [26] M. Schröter, D. I. Goldman, H. L. Swinney, *Phys. Rev. E* **71**, 030301(R) (2005).
- [27] F. Léchenault, O. Dauchot and E. Bertin, *J. Stat. Mech.*, P07009 (2006).
- [28] V. S. Kumar and V. Kumaran, *Journal of Chemical Physics* **123**, 074502 (2005).
- [29] T. Aste, A. V. Anikeenko and N. N. Medvedev, *Phys. Rev E* **77**, 031101 (2008)
- [30] C. E. Shannon, *Bell Sys. Tech. J.* **27**, 379 (1948).
- [31] R. L. C. Vink and G. T. Barkema, *Phys. Rev. Lett.* **89**, 076405 (2002).
- [32] V. S. Kumar and V. Kumaran, *Journal of Chemical Physics* **123**, 114501 (2005).
- [33] J. Brujić, C. Song, P. Wang, C. Briscoe, G. Marty, and H. A. Makse, *Phys. Rev. Lett.* **98**, 248001 (2007).
- [34] B. D. McKay, Nauty user's guide (version 1.5), Tech. Rep. TR-CS-90-02, Australian National University (1990).
- [35] P. Rombouts, Masters Thesis, Institute for Theoretical Physics, Utrecht University, (2004)
- [36] G. Parisi and Zamponi, *J. Chem. Phys.* **123**, 144501 (2005), arXiv:0802.2180
- [37] J. Brujić, P. Wang, D. Johnson, O. Sindt, and H. A. Makse, *Phys. Rev. Lett.* **95**, 128001 (2005).
- [38] H. A. Makse and J. Kurchan, *Nature* **415**, 614 (2002).
- [39] S.F. Edwards, *Physica A*, **353**, 114 (2005).
- [40] R. Blumenfeld, On Entropic Characterization of Granular Materials in *Lecture Notes in Complex Syetems Vol 8: Granular and Complex Materials*, **43-53** (2007)
- [41] S. Henkes, B. Chakraborty, *Phys. Rev. Lett.* **95**, 198002 (2005).
- [42] S. Ostojic, E. Somfai, B. Nienhuis, *Nature* **439**, 828 (2006).
- [43] J. H. Snoeijer, T. J. H. Vlugt, M. van Hecke, W. van Saarloos, *Phys. Rev. Lett.* **92**, 054302 (2004).
- [44] E. Bertin, O. Dauchot, and M. Droz, *Phys. Rev. Lett.* **93**, 230601 (2004).
- [45] L. D. Landau and E. M. Lifshitz, *Statistical Physics* (Pergamon, NY, 1970).
- [46] F. H Stillinger, *Science* **267**, 1935-1939 (1995).
- [47] T. Aste and T. Di Matteo, *Phys. Rev. E* **77**, 021309 (2008)